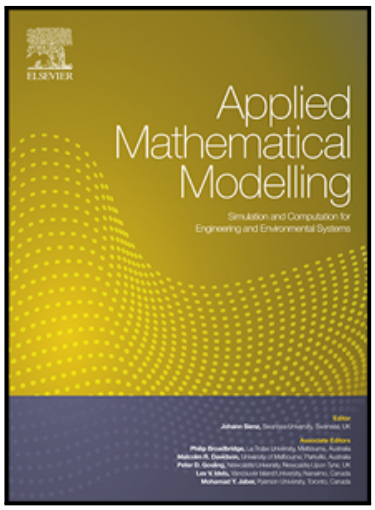

On wave propagation in two-dimensional functionally graded porous rotating nano-beams using a general nonlocal higher-order beam model

S. Faroughi , A. Rahmani , M.I. Friswell

PII: S0307-904X(19)30723-1
DOI: https://doi.org/10.1016/j.apm.2019.11.040
Reference: APM 13170

To appear in: *Applied Mathematical Modelling*

Received date: 27 July 2019
Revised date: 6 November 2019
Accepted date: 26 November 2019

Please cite this article as: S. Faroughi , A. Rahmani , M.I. Friswell , On wave propagation in two-dimensional functionally graded porous rotating nano-beams using a general nonlocal higher-order beam model, *Applied Mathematical Modelling* (2019), doi: https://doi.org/10.1016/j.apm.2019.11.040

Highlights:

- For the first time, the comprehensive wave propagation analysis of 2D-FG rotating nanobeams with porosity is considered
- General nonlocal theory is used to establish the governing equation which exhibits softening and hardening behavior
- Reddy's beam theory is applied to model the effects of the higher-order transverse shear strains on the wave propagation
- The effects of material variation, porosity, and the length to thickness ratio on the wave propagation are discussed

On wave propagation in two-dimensional functionally graded porous rotating nano-beams using a general nonlocal higher-order beam model

S. Faroughi, A. Rahmani, M.I. Friswell*

Faculty of Mechanical Engineering, Urmia University of Technology, Urmia, Iran
College of Engineering, Swansea University, Swansea, UK

Abstract

This paper studies the wave propagation of two-dimensional functionally graded (2D-FG) porous rotating nano-beams for the first time. The rotating nano-beams are made of two different materials, and the material properties of the nano-beams alter both in the thickness and length directions. The general nonlocal theory (GNT) in conjunction with Reddy's beam model are employed to formulate the size-dependent model. The GNT efficiently models the dispersions of acoustic waves when two independent nonlocal fields are modelled for the longitudinal and transverse acoustic waves. The governing equations of motion for the 2D-FG porous rotating nano-beams are established using Hamilton's principle as a function of the axial force due to centrifugal stiffening and displacement. The analytic solution is applied to obtain the results and solve the governing equations. The effect of the features of different parameters such as functionally graded power indexes, porosity, angular velocity, and material variation on the wave propagation characteristics of the rotating nano-beams are discussed in detail.

Keywords: Wave Propagation; General Nonlocal Theory; Reddy's Beam Model; 2D-FG Beam; Rotating Nano-Beam

* Corresponding author, m.i.friswell@swansea.ac.uk

1. Introduction

Nanostructures and nanotechnologies have been progressively employed in nano-electro-mechanical systems (NEMS) owing to their exceptional mechanical and physical features, and the investigation of nanostructures has been the subject of much research. The efficiency of nano-beams is one of the key characteristics of nano/micro structures.

Continuum mechanics (CM) has been shown to be a consistent and suitable method to explore the mechanical performance of structures at numerous length and time scales. Eringen's nonlocal theory (ENT) is the widely employed CM theory that considers size effects with exceptional accuracy to simulate size-dependent structures. ENT has been extensively employed to study nanostructures. Reddy [1] expressed the Euler–Bernoulli, Timoshenko, Reddy and Levinson beam models by applying ENT. Wang and Liew [2] studied the static behaviour of small-scale structures corresponding to nonlocal CM considering Euler–Bernoulli (EBT) and Timoshenko (TBT) beam models.

Strain gradient theory (SGT) is a CM theory that is also used to study nano-beams. Sourki and Hosseini [3] proposed the vibrational model of a nano-beam containing surface effects. Karami et al. [4] employed the nonlocal SGT model to investigate hydrothermal wave propagation in viscoelastic graphene and nano-plate porous heterogeneous materials under magnetic fields. She et al. [5] applied the nonlocal SGT model to study wave propagation in nano-tubes. Lu et al. [6, 7] used a new beam model to study the vibration and buckling of nano-beams. Moreover, Li et al. [8] examined the vibrational performances of nano-beam.

Functionally graded materials (FGMs) are composed of metal and ceramic and have a continuous material variation from one surface to the other which is designed to attain desirable and feasible features. In recent decades, applications of FGMs have significantly increased and have been considered by many researchers. Specifically, the mechanical behaviour of micro/nano structures made of FGMs, such as bending, buckling, vibration, and wave propagation, have been assessed by many scientists. Ebrahimi and Barati considered the vibrational behaviour of functionally graded (FG) nano-beams [9] in thermal environments. Al-Basyouni et al. [10] employed modified couple stress (MCS) theory to consider the bending and vibrational behaviour of FG micro-beams. Mehralian and Beni [11] presented the vibrational behaviour of bimorph

functionally graded piezoelectric nano-shells based on nonlocal strain gradient theory. Also, Mehralian et al. [11, 12] illustrated buckling analysis of functionally graded piezoelectric cylindrical nano shells on the basis of a new modified couple stress theory.

Zeighampour and Beni [13] studied the vibrational behaviour of axially functionally graded nano-beams resting on elastic foundations employing the strain gradient theory with the Euler–Bernoulli beam model.

Ebrahimi et al. [14] investigated wave propagation in inhomogeneous FG nano-beams via SGT and higher order beam models considering the effects of the thermal environment. Li et al. [15] applied nonlocal SGT and Euler-Bernoulli beam theory to investigate the wave propagation in FG nano-beams. Moreover Nejad and Hadi [16], studied the free vibration of FG Euler–Bernoulli nano-beams. Ma et al. [17] presented wave propagation in magneto-electro-elastic nano-beams based on Timoshenko beam theory. Khorshidi and Shariati [18] used MCS and Reddy's beam theories to model bending wave propagation in nano-beams. Arefi and Zenkour [19, 20] considered the wave propagation in FG and FG magneto-electro-elastic material nano-beams using the Timoshenko beam model. Zeighampour et al. [21] investigated the wave propagation problem in viscoelastic single walled carbon nanotubes. The considered simultaneous effects of the material length scale parameter and the nonlocal coefficient. They employed the nonlocal strain gradient and shell theory to establish the model. They also reported wave propagation analysis of composite laminated cylindrical micro-shells and considered the effect of the fibre angle in the layers on the phase velocity [22].

Various and extensive engineering applications of porous materials are due to their distinguishing properties such as low electrical and thermal conductivity, low specific weight and impressive energy dissipation capacity. Some important applications of porous materials are reported in the water and oil industries, biomedical materials, and aerospace, automotive, railway and marine structural components [23, 24].

Renault et al. [25] used the frequency response functions of a free–free bending beam to estimate the visco-elastic parameters of damped porous materials. Barati [26, 27] established a general bi-Helmholtz nonlocal strain gradient (SG) model to study wave propagation in porous nano-beams.

The combination of porous materials with FGMs is a creative and effective topic that has attracted original research in recent years. According to the literature survey, there are some investigations on FG porous materials, although most current studies

consider only static behaviours such as bending or buckling analysis. One of the most important applications of FG porous materials is related to their outstanding capability in energy absorption [28, 29]. Hence, consideration of the dynamical response, such as the vibration and wave propagation behaviour, of FG porous materials should be investigated.

Chen et al. [30] studied the free and forced vibrational behaviour of FG porous Timoshenko beams. Shafiei et al. [31] presented the vibration analysis of 2D-FG nano/micro beams with two different kinds of porous materials. They used Eringen's and the modified couple stress theories with the Timoshenko beam model. Mirjavadi et al. [32, 33] investigated the thermal vibrational behaviour of 2D-FG porous Timoshenko micro and nano beams using MCST and ENT.

Jouneghani et al. [34] studied the bending behaviour of FG porous nano-beams under hygro-thermo-mechanical loading. They used Eringen's theory to extract the model. Eltaher et al. [35] analysed the mechanical vibration and bending of FG porous nano-beams by applying nonlocal continuum theory and a modified porosity model. They used Euler beam theory to extract the model and the finite element method (FEM) to solve the problem. Liu et al. [36] presented the vibration analysis of FG porous magneto-electro-viscoelastic nano-beams on the basis of nonlocal Timoshenko beam theory and the Kelvin-Voigt viscoelastic model. She et al. [37] utilized nonlocal SG and Reddy's beam theories to evaluate the wave propagation performance of FG porous nano-beams. More recently, Karami and Janghorban [38] reported the free vibration analysis of porous nanotubes using the Timoshenko beam model and nonlocal strain gradient theory. Ebrahimi-Nejad et al. [39] investigated the vibrational behaviour of 2D-FG porous nano-beams subjected to hygro-thermo-mechanical loading on the basis of the Euler-Bernoulli beam model and Eringen's theory. Recently, Ebrahimi et al. [40-42] performed an extensive study on the wave dispersion in FG porous nano-beams considering the coupling effects between density and Young's modulus in porous materials, employing a new two-step porosity-dependent homogenization scheme and nonlocal strain gradient inhomogeneous nano-beams.

Rotating nanostructures, including molecular bearings, nanogears, nanoturbines and multiple-gear systems, are the subject of much research. Their accurate design requires the examination of the vibration and wave propagation of nano-machines. Recently, Mohammadi et al. [43] studied the vibrational behaviour of a rotating nano-beam embedded in a Pasternak elastic medium with thermal effects. Ebrahimi and

Shafei [44] used Eringen's nonlocal theory to study the vibrational behaviour of rotating FG nano-beams. Ebrahimi and Haghi [45] studied the wave propagation performance of rotating FG temperature-dependent nanoscale beams under thermal loading based on a nonlocal SG stress field.

Based on this literature review, the investigation of wave propagation in FG nano-beams and rotating nano-beams have only considered transverse and longitudinal waves and have used Eringen's nonlocal theory (ENT), strain gradient (SG) theory, and couple stress (CS) theory. Moreover, there are no studies on the wave propagation in bi-directional functionally graded (2D-FG) porous nano-beams and rotating nano-beams and GNT.

Recently, Shaat [46, 47] has revealed that ENT has some serious limitations for materials with different nonlocal transverse and longitudinal behaviours. Hence, the GNT was proposed by Shaat [46, 47]. The GNT is established on the basis of the difference between the shear and normal strains in the nonlocal fields. The transverse and the longitudinal acoustic dispersions of materials can be considered simultaneously in GNT. Also, GNT can model the effect of Poisson's ratio on the mechanical behaviour of different materials [48].

The literature review also highlights that there are no studies on the wave propagation behaviour of a rotating nano-beam made of two dimensional functionally graded (2D-FG) porous materials. Therefore, in this paper, the wave propagation behaviour of 2D-FG rotating nano-beams with porosities is considered on the basis of GNT and Reddy's beam model for the first time. For this purpose, GNT is used to model the interatomic interactions. The 2D-FG porous material model is considered due to the porosity of the material which includes the effects of FG power indexes along the thickness (nz) and the length (nx) directions. An analytical approach is used to solve the governing equation and to extract the results. Finally, a parametric study is performed to investigate the effects of the properties of many parameters, such as porosity and 2D-FG power indexes, on the wave propagation in 2D rotating nano-beams.

2. Governing Equations

2.1. 2D-FG Materials

The 2D-FG rotating nano-beam consists of ceramic and metal with changing material volume fraction along the z and x directions, as shown in Fig. 1, where the material

configuration alters along both the axis and the thickness directions. Therefore, the mechanical properties of the nano-beam, such as Lame's constants, alter along longitudinal (*x*-axis) and thickness (*z*-axis) directions.

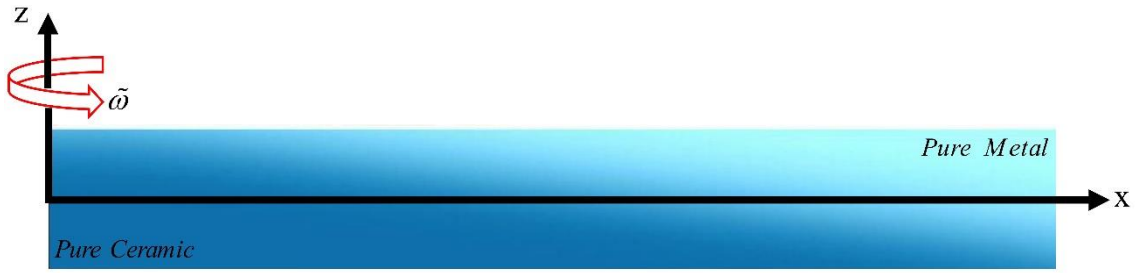

Fig. 1. Schematic of the material distribution

Although the porous 2D-FG nano-beam can be assumed to have even and uneven porosity distributions across thickness of the beam, in present study only even porosity distributions is considered. Lame's constants and the mass density for the even distribution of porosities inside the material are given by [31]:

$$\lambda(x,z) = \lambda_m + (\lambda_c - \lambda_m)\left(\frac{1}{2} + \frac{z}{h}\right)^{nz}\left(\frac{x}{L}\right)^{nx} - \frac{\gamma}{2}(\lambda_c + \lambda_m)$$
$$\mu(x,z) = \mu_m + (\mu_c - \mu_m)\left(\frac{1}{2} + \frac{z}{h}\right)^{nz}\left(\frac{x}{L}\right)^{nx} - \frac{\gamma}{2}(\mu_c + \mu_m) \quad (1)$$
$$\rho(x,z) = \rho_m + (\rho_c - \rho_m)\left(\frac{1}{2} + \frac{z}{h}\right)^{nz}\left(\frac{x}{L}\right)^{nx} - \frac{\gamma}{2}(\rho_c + \rho_m)$$

The $(\ )_m$ and $(\ )_c$ subscripts denote the metal and ceramic properties respectively. nx and nz denote the power law indexes and γ is the porosity volume fraction. The material of the beam is 100% ceramic when $\gamma = 0$, $nx = 0$ and $nz = 0$.

The displacement field at any point of the beam can be written on the basis of the third-order shear deformation beam theory (Reddy) as:

$$u_x(x,z,t) = u^0(x) + z\psi(x) - \frac{4}{3h^2}z^3\left(\psi + \frac{\partial w}{\partial x}\right) \quad (2)$$
$$u_z(x,z,t) = w(x)$$

where u^0, w and ψ represent the longitudinal displacement, transverse displacement and rotation of the cross section at *x*, respectively. The strains of the Reddy beam model are defined as follows:

$$\varepsilon_{xx}(x,z,t) = \frac{\partial u^0(x)}{\partial x} + z\frac{\partial \psi(x)}{\partial x} - \frac{4}{3h^2}z^3\left(\frac{\partial \psi(x)}{\partial x} + \frac{\partial^2 w(x)}{\partial x^2}\right)$$
$$= \varepsilon_{xx}^{(0)} + z\varepsilon_{xx}^{(1)} + z^3\varepsilon_{xx}^{(3)} \quad (3)$$
$$\gamma_{xz}(x,z,t) = \frac{\partial w(x)}{\partial x} + \psi(x) - \frac{4}{h^2}z^2\left(\psi + \frac{\partial w}{\partial x}\right) = \gamma_{xz}^{(0)} + z^2\gamma_{xz}^{(2)}$$

Hamilton's principle is employed to establish the governing equations and is given by:

$$\int_0^t \delta(U - T + V)dt = 0 \quad (4)$$

where T and U are the kinetic and strain energies, respectively. Also, V indicates the work done by the external forces. Now, the variation of strain energy can be computed as:

$$\delta U = \int_v (\sigma_{xx}\delta\varepsilon_{xx} + \tau_{xz}\delta\gamma_{xz})dv \quad (5)$$

Substituting Eq. (3) into Eq. (5) yields

$$\delta U = \int_0^L \left(Q\delta\varepsilon_{xx}^{(0)} + M\varepsilon_{xx}^{(1)} + E\varepsilon_{xx}^{(3)} + F\gamma_{xz}^{(0)} + R\gamma_{xz}^{(2)}\right)dx \quad (6)$$

where

$$Q = \int_A \sigma_{xx}dA; \quad M = \int_A z\sigma_{xx}dA; \quad E = \int_A z^3\sigma_{xx}dA; \quad F = \int_A \tau_{xz}dA;$$
$$R = \int_A z^2\tau_{xz}dA \quad (7)$$

The first variation of the work done by the applied forces can be evaluated as:

$$\delta V = \int_0^L \left(T(x)\frac{\partial w}{\partial x}\frac{\partial \delta w}{\partial x} + q\delta w + f\delta u^0 - N\delta\varepsilon_{xx}^{(0)} - \widetilde{M}\frac{\partial \delta\psi}{\partial x} + \frac{4}{3h^2}E\frac{\partial^2 \delta w}{\partial x^2}\right.$$
$$\left. - \tilde{F}\delta\gamma_{xz}^{(0)}\right)dx \quad (8)$$

where $\widetilde{M} = M - \frac{4}{3h^2}E$, $\tilde{F} = F - \frac{4}{h^2}R$ and $T(x)$ is the external applied axial force due to the rotation and q and f indicate the transverse and axial distributed loads. The axial force due to centrifugal stiffening due to rotation is given as

$$T(x) = T(x) = b\int_{x}^{L}\int_{-h/2}^{h/2}\rho(x,z)\Omega^2\, x dz dx \tag{9}$$

where ρ is the mass density, A is the beam cross-section area and Ω is the rotation speed. The variation of the virtual kinetic energy for the homogeneous nano-beam can be expressed as:

$$\begin{aligned}\delta K = \int_0^L \Bigg(& J_0\left(\frac{\partial u^0}{\partial t}\frac{\partial \delta u^0}{\partial t} + \frac{\partial w}{\partial t}\frac{\partial \delta w}{\partial t}\right) + J_1\left(\frac{\partial u^0}{\partial t}\frac{\partial \delta \psi}{\partial t} + \frac{\partial \psi}{\partial t}\frac{\partial \delta}{\partial t}\right) + J_2\frac{\partial \psi}{\partial t}\frac{\partial \delta \psi}{\partial t} \\ & + \frac{4}{3h^2}\Bigg[-J_3\frac{\partial u}{\partial t}\left(\frac{\partial \delta \psi}{\partial t} + \frac{\partial^2 \delta w}{\partial x \partial t}\right) - J_3\frac{\partial \delta u}{\partial t}\left(\frac{\partial \psi}{\partial t} + \frac{\partial^2 \delta w}{\partial x \partial t}\right) \\ & - J_4\frac{\partial \psi}{\partial t}\left(\frac{\partial \delta \psi}{\partial t} + \frac{\partial^2 \delta w}{\partial x \partial t}\right) - J_4\frac{\partial \delta \psi}{\partial t}\left(\frac{\partial \psi}{\partial t} + \frac{\partial^2 w}{\partial x \partial t}\right) \\ & + \frac{4}{3h^2}J_6\left(\frac{\partial \psi}{\partial t} + \frac{\partial^2 w}{\partial x \partial t}\right)\left(\frac{\partial \delta \psi}{\partial t} + \frac{\partial^2 \delta w}{\partial x \partial t}\right)\Bigg]\Bigg) dx\end{aligned} \tag{10}$$

where J_0, J_1, J_2, J_3, J_4 and J_6 are the mass inertias and calculated as:

$$(J_0, J_1, J_2, J_3, J_4, J_6) = \int_A \rho(x,z)(1, z, z^2, z^3, z^4, z^6)\, dA \tag{11}$$

Substituting Eqs. (6), (8) and (10) into Eq. (4) and setting the coefficients of δu^0, δw and $\delta \psi$ to zero, the subsequent Euler–Lagrange equation can be obtained as:

$$\begin{aligned} & \frac{\partial Q}{\partial x} + f - J_0\frac{\partial^2 u^0}{\partial t^2} - \hat{J}_1\frac{\partial^2 \psi}{\partial t^2} + \frac{4}{3h^2}J_3\frac{\partial^3 w}{\partial x \partial t^2} = 0 \\ & \frac{\partial \tilde{M}}{\partial x} - \tilde{F} - \hat{J}_1\frac{\partial^2 u^0}{\partial t^2} - \hat{J}_2\frac{\partial^2 \psi}{\partial t^2} + \frac{4}{3h^2}\hat{J}_4\left(\frac{\partial^2 \psi}{\partial t^2} + \frac{\partial^3 w}{\partial x \partial t^2}\right) = 0 \\ & \frac{\partial \tilde{F}}{\partial x} + q + \frac{\partial}{\partial x}\left(T(x)\frac{\partial w}{\partial x}\right) + \frac{4}{3h^2}\frac{\partial^2 E}{\partial x^2} - J_0\frac{\partial^2 w}{\partial t^2} - \frac{4}{3h^2}J_3\frac{\partial^3 u}{\partial x \partial t^2} - \frac{4}{3h^2}J_4\frac{\partial^3 \psi}{\partial x \partial t^2} \\ & \qquad + \left(\frac{4}{3h^2}\right)^2 J_6\left(\frac{\partial^3 \psi}{\partial x \partial t^2} + \frac{\partial^4 w}{\partial x^2 \partial t^2}\right) = 0 \end{aligned} \tag{12a}$$

$$\begin{aligned} & (Q - N)\delta u = 0 \quad x = 0, L \\ & \tilde{M}\delta \psi = 0 \qquad x = 0, L \\ & \frac{8}{3h^2}\frac{\partial E}{\partial x} + 2\tilde{F} + T(x)\frac{\partial w}{\partial x} - \frac{4}{3h^2}J_3\frac{\partial^2 u}{\partial t^2} - \frac{4}{3h^2}\hat{J}_4\frac{\partial^2 \psi}{\partial t^2} + \left(\frac{4}{3h^2}\right)^2 J_6\frac{\partial^3 w}{\partial x \partial t^2} = 0 \quad x = 0, L \end{aligned} \tag{12b}$$

where $\hat{J}_1 = J_1 - \frac{4}{3h^2}J_3$, $\hat{J}_2 = J_2 - \frac{4}{3h^2}J_4$ and $\hat{J}_4 = J_4 - \frac{4}{3h^2}J_6$

2.2. Review of General Nonlocal Theory

A novel nonlocal theory named GNT was proposed by Shaat et al. [46, 47] which was developed on the basis of the difference between the shear and normal strains in the nonlocal fields. They introduced new insights in the applicability of Eringen's nonlocal theory. They showed that conventional ENT cannot simultaneously fit shear (transverse) and longitudinal acoustic dispersion in materials. Therefore, they developed the general nonlocal theory that compensates for these shortcomings in conventional ENT and can reflect both hardening and softening behaviours of the material. Accordingly, the best theory to illustrate the wave propagation behaviour of materials in this study is GNT.

Unlike Eringen's nonlocal theory (ENT), the general nonlocal theory (GNT) utilizes two different nonlocal factors. Based on the GNT [47], the nonlocal stress field at each point in the Equilibrium equation can be expressed in the following form:

$$\sigma_{ji,j}(\boldsymbol{x},t) + f_i(\boldsymbol{x},t) = \rho \frac{d^2 u_i(\boldsymbol{x},t)}{dt^2} \tag{13}$$

with the constitutive equations:

$$\sigma_{ji}(\boldsymbol{x}) = \int_V \left(\lambda\, \beta_1(|\boldsymbol{x}' - \boldsymbol{x}|)\varepsilon_{rr}(\boldsymbol{x}')\delta_{ij} + 2\mu\beta_2(|\boldsymbol{x}' - \boldsymbol{x}|)\varepsilon_{ij}(\boldsymbol{x}')\right) dV' \tag{14}$$

σ_{ji} denotes the nonlocal stress field that is expressed in terms of the two different nonlocal factors, $\beta_1(|\boldsymbol{x}' - \boldsymbol{x}|)$ and $\beta_2(|\boldsymbol{x}' - \boldsymbol{x}|)$. Also, $\varepsilon_{ij} = \frac{1}{2}\left(u_{i,j} + u_{j,i}\right)$ defines the nonlocal strain field and u_i is the displacement field. f_i is the body force, ρ is the mass density, and t is the time.

According to the GNT, to create the differential form of the constitutive equations of the nonlocal theory, two differential operators are applied as follows [47]:

$$\mathcal{L}_1\beta_1(|\mathbf{x}' - \mathbf{x}|) = \delta(|\mathbf{x}' - \mathbf{x}|) \text{ and } \mathcal{L}_2\beta_2(|\mathbf{x}' - \mathbf{x}|) = \delta(|\mathbf{x}' - \mathbf{x}|) \tag{15}$$

where δ is the Dirac-delta, and $\mathcal{L}_1$ and $\mathcal{L}_2$ are differential operators, for example $\mathcal{L}_1 = (1 - \epsilon_1\boldsymbol{\nabla}^2)$ and $\mathcal{L}_2 = (1 - \epsilon_2\boldsymbol{\nabla}^2)$, where the Laplacian gradient operator is $\boldsymbol{\nabla}^2 = \frac{\partial^2}{\partial x^2}$, and ϵ_1 and ϵ_2 denote the constant nonlocal coefficients which are dependent on the lattice constant.

Accordingly, the differential equation for the general nonlocal model is represented as [47]:

$$(1-\epsilon_1\nabla^2)(1-\epsilon_2\nabla^2)\sigma_{(ji)}(\mathbf{x}) = \lambda(1-\epsilon_2\nabla^2)\varepsilon_{rr}(\mathbf{x})\delta_{ij} + 2\mu(1-\epsilon_1\nabla^2)\varepsilon_{ij}(\mathbf{x}) \tag{16}$$

where λ and μ are Lame's constants of the material. According to the constitutive equations represented in Eq. (16), the transverse and longitudinal acoustic dispersions of the material can be considered simultaneously in GNT and it demonstrates the superiority of GNT versus Eringen's nonlocal theory [46, 47]. GNT can also reflect both the softening and hardening performances of materials due to the explanation of the nonlocal parameters. Here, the GNT is used to investigate the effects of the long-range interatomic interactions on the dispersion of acoustic waves of porous rotating nano-beams.

According to the GNT, the following constitutive relations are attained:

$$\begin{aligned}(1-\epsilon_1\nabla^2)(1-\epsilon_2\nabla^2)\sigma_{xx} &= \lambda(1-\epsilon_2\nabla^2)(\varepsilon_{xx}) + 2\mu(1-\epsilon_1\nabla^2)\varepsilon_{xx}\\ (1-\epsilon_1\nabla^2)(1-\epsilon_2\nabla^2)\sigma_{xy} &= 2\mu(1-\epsilon_1\nabla^2)\gamma_{xy}\end{aligned} \tag{17}$$

To create the governing equations of motion for the rotating nano-beam, first and according to Eq. (3), the force strain, N_{ij}, and the moment strain, M_{ij} , are defined in terms of the displacements as:

$$\begin{aligned}&(1-\epsilon_1\nabla^2)(1-\epsilon_2\nabla^2)Q\\ &\quad= (1-\epsilon_2\nabla^2)\left(A_{11}\frac{\partial u}{\partial x} + (B_{11}-\frac{4}{3h^2}E_{11})\frac{\partial\psi}{\partial x} - \frac{4}{3h^2}E_{11}\frac{\partial^2 w(x)}{\partial x^2}\right)\\ &\quad+ 2(1-\epsilon_1\nabla^2)\left(\bar{A}_{11}\frac{\partial u}{\partial x} + (\bar{B}_{11}-\frac{4}{3h^2}\bar{E}_{11})\frac{\partial\psi}{\partial x} - \frac{4}{3h^2}\bar{E}_{11}\frac{\partial^2 w(x)}{\partial x^2}\right)\end{aligned} \tag{18-a}$$

$$\begin{aligned}&(1-\epsilon_1\nabla^2)(1-\epsilon_2\nabla^2)M\\ &\quad= (1-\epsilon_2\nabla^2)\left(B_{11}\frac{\partial u}{\partial x} + (D_{11}-\frac{4}{3h^2}F_{11})\frac{\partial\psi}{\partial x} - \frac{4}{3h^2}F_{11}\frac{\partial^2 w(x)}{\partial x^2}\right)\\ &\quad+ 2(1-\epsilon_1\nabla^2)\left(\bar{B}_{11}\frac{\partial u}{\partial x} + (\bar{D}_{11}-\frac{4}{3h^2}\bar{F}_{11})\frac{\partial\psi}{\partial x} - \frac{4}{3h^2}\bar{F}_{11}\frac{\partial^2 w(x)}{\partial x^2}\right)\end{aligned} \tag{18-b}$$

$$\begin{aligned}&(1-\epsilon_1\nabla^2)(1-\epsilon_2\nabla^2)E\\ &\quad= (1-\epsilon_2\nabla^2)\left(E_{11}\frac{\partial u}{\partial x} + (F_{11}-\frac{4}{3h^2}H_{11})\frac{\partial\psi}{\partial x} - \frac{4}{3h^2}H_{11}\frac{\partial^2 w(x)}{\partial x^2}\right)\\ &\quad+ 2(1-\epsilon_1\nabla^2)\left(\bar{E}_{11}\frac{\partial u}{\partial x} + (\bar{F}_{11}-\frac{4}{3h^2}\bar{H}_{11})\frac{\partial\psi}{\partial x} - \frac{4}{3h^2}\bar{H}_{11}\frac{\partial^2 w(x)}{\partial x^2}\right)\end{aligned} \tag{18-c}$$

$$(1-\epsilon_1\nabla^2)(1-\epsilon_2\nabla^2)F = 2(1-\epsilon_1\nabla^2)\left(A_{12}-\frac{4}{h^2}D_{12}\right)\left(\psi+\frac{\partial w}{\partial x}\right) \tag{18-d}$$

$$(1-\epsilon_1\nabla^2)(1-\epsilon_2\nabla^2)R = 2(1-\epsilon_1\nabla^2)\left(D_{12}-\frac{4}{h^2}F_{12}\right)\left(\psi+\frac{\partial w}{\partial x}\right) \tag{18-e}$$

where the cross sectional rigidities are defined by:

$$(A_{11}, B_{11}, D_{11}, E_{11}, F_{11}, H_{11}) = \int_A \lambda(x,z)(1, z, z^2, z^3, z^4, z^6)dA \tag{19}$$

$$(\bar{A}_{11}, \bar{B}_{11}, \bar{D}_{11}, \bar{E}_{11}, \bar{F}_{11}, \bar{H}_{11}) = \int_A \mu(x,z)(1, z, z^2, z^3, z^4, z^6)dA$$

$$(A_{12}, D_{12}, F_{12}) = \int_A \mu(x,z)(1, z^2, z^4)dA$$

Then, $\widetilde{M}$ and $\tilde{F}$ are obtained by combining Eqs. (18-b) and (18-c) and (18-d) and (18-e) respectively, as follows:

$$\begin{aligned}
&(1-\epsilon_1\boldsymbol{\nabla}^2)(1-\epsilon_2\boldsymbol{\nabla}^2)\widetilde{M} \\
&\quad = (1-\epsilon_2\boldsymbol{\nabla}^2)\left(\alpha_{11}\frac{\partial u}{\partial x} + \beta_{11}\frac{\partial \psi}{\partial x} - \frac{4}{3h^2}\delta_{11}\left(\frac{\partial \psi}{\partial x} + \frac{\partial^2 w(x)}{\partial x^2}\right)\right) \\
&\quad + 2(1-\epsilon_1\boldsymbol{\nabla}^2)\left(\bar{\alpha}_{11}\frac{\partial u}{\partial x} + \bar{\beta}_{11}\frac{\partial \psi}{\partial x} - \frac{4}{3h^2}\bar{\delta}_{11}\left(\frac{\partial \psi}{\partial x} + \frac{\partial^2 w(x)}{\partial x^2}\right)\right) \\
&\quad (1-\epsilon_1\boldsymbol{\nabla}^2)(1-\epsilon_2\boldsymbol{\nabla}^2)\tilde{F} = 2\mu(1-\epsilon_1\boldsymbol{\nabla}^2)\bar{A}\left(\psi + \frac{\partial w}{\partial x}\right)
\end{aligned} \tag{20}$$

where

$$\begin{aligned}
&\alpha_{11} = B_{11} - \frac{4}{3h^2}E_{11}, \beta_{11} = D_{11} - \frac{4}{3h^2}F_{11}, \delta_{11} = F_{11} - \frac{4}{3h^2}H_{11} \\
&\bar{\alpha}_{11} = \bar{B}_{11} - \frac{4}{3h^2}\bar{E}_{11}, \bar{\beta}_{11} = \bar{D}_{11} - \frac{4}{3h^2}\bar{F}_{11}, \bar{\delta}_{11} = \bar{F}_{11} - \frac{4}{3h^2}\bar{H}_{11} \\
&\bar{A} = A_{12} - \frac{4}{h^2}D_{12} - \frac{4}{h^2}D_{12} + \left(\frac{4}{h^2}\right)^2 F_{12}
\end{aligned} \tag{21}$$

Then, by multiplying Eq. (12) by $(1-\epsilon_1\boldsymbol{\nabla}^2)(1-\epsilon_2\boldsymbol{\nabla}^2)$ and utilizing Eqs. (18) and (20) the governing equations of motion of the rotating nonlocal beam are obtained in term of the displacements in the following form:

$$\begin{aligned}
&(-\varepsilon_2 A_{11} - 2\varepsilon_1\bar{A}_{11})\frac{\partial^4 u}{\partial x^4} + (-2\varepsilon_2\frac{\partial A_{11}}{\partial x} - 4\varepsilon_1\frac{\partial \bar{A}_{11}}{\partial x})\frac{\partial^3 u}{\partial x^3} + (A_{11} + 2\bar{A}_{11} - \varepsilon_2\frac{\partial^2 A_{11}}{\partial x^2} - 2\varepsilon_1\frac{\partial^2 \bar{A}_{11}}{\partial x^2})\frac{\partial^2 u}{\partial x^2} + \\
&(-\varepsilon_2\alpha_{11} - 2\varepsilon_1\bar{\alpha}_{11})\frac{\partial^4 \psi}{\partial x^4} + (-2\varepsilon_2\frac{\partial \alpha_{11}}{\partial x} - 4\varepsilon_1\frac{\partial \bar{\alpha}_{11}}{\partial x})\frac{\partial^3 \psi}{\partial x^3} + (\alpha_{11} + 2\bar{\alpha}_{11} - \varepsilon_2\frac{\partial^2 \alpha_{11}}{\partial x^2} - 2\varepsilon_1\frac{\partial^2 \bar{\alpha}_{11}}{\partial x^2})\frac{\partial^2 \psi}{\partial x^2} + \\
&\bar{\kappa}(-\varepsilon_2 E_{11} - 2\varepsilon_1\bar{E}_{11})\frac{\partial^5 w}{\partial x^5} + \bar{\kappa}(-2\varepsilon_2\frac{\partial E_{11}}{\partial x} - 4\varepsilon_1\frac{\partial \bar{E}_{11}}{\partial x})\frac{\partial^4 w}{\partial x^4} + \bar{\kappa}(E_{11} + 2\bar{E}_{11} - \varepsilon_2\frac{\partial^2 E_{11}}{\partial x^2} - 2\varepsilon_1\frac{\partial^2 \bar{E}_{11}}{\partial x^2})\frac{\partial^3 w}{\partial x^3} + \\
&[-J_0 + (\varepsilon_1+\varepsilon_2)\frac{\partial^2 J_0}{\partial x^2} - \varepsilon_1\varepsilon_2\frac{\partial^4 J_0}{\partial x^4}]\frac{\partial^2 u}{\partial t^2} + [2(\varepsilon_1+\varepsilon_2)\frac{\partial J_0}{\partial x} - 4\varepsilon_1\varepsilon_2\frac{\partial^3 J_0}{\partial x^3}]\frac{\partial^3 u}{\partial x\,\partial t^2} + \\
&[(\varepsilon_1+\varepsilon_2)J_0 - 6\varepsilon_1\varepsilon_2\frac{\partial^2 J_0}{\partial x^2}]\frac{\partial^4 u}{\partial x^2\,\partial t^2} + [-4\varepsilon_1\varepsilon_2\frac{\partial J_0}{\partial x}]\frac{\partial^5 u}{\partial x^3\,\partial t^2} + [-\varepsilon_1\varepsilon_2 J_0]\frac{\partial^6 u}{\partial x^4\,\partial t^2} + \\
&[-\hat{J}_1 + (\varepsilon_1+\varepsilon_2)\frac{\partial^2 \hat{J}_1}{\partial x^2} - \varepsilon_1\varepsilon_2\frac{\partial^4 \hat{J}_1}{\partial x^4}]\frac{\partial^2 \psi}{\partial t^2} + [2(\varepsilon_1+\varepsilon_2)\frac{\partial \hat{J}_1}{\partial x} - 4\varepsilon_1\varepsilon_2\frac{\partial^3 \hat{J}_1}{\partial x^3}]\frac{\partial^3 \psi}{\partial x\,\partial t^2} + \\
&[(\varepsilon_1+\varepsilon_2)\hat{J}_1 - 6\varepsilon_1\varepsilon_2\frac{\partial^2 \hat{J}_1}{\partial x^2}]\frac{\partial^4 \psi}{\partial x^2\,\partial t^2} + [-4\varepsilon_1\varepsilon_2\frac{\partial \hat{J}_1}{\partial x}]\frac{\partial^5 \psi}{\partial x^3\,\partial t^2} + [-\varepsilon_1\varepsilon_2\hat{J}_1]\frac{\partial^6 \psi}{\partial x^4\,\partial t^2} + \\
&\bar{\kappa}[-J_3 + (\varepsilon_1+\varepsilon_2)\frac{\partial^2 J_3}{\partial x^2} - \varepsilon_1\varepsilon_2\frac{\partial^4 J_3}{\partial x^4}]\frac{\partial^3 w}{\partial x\,\partial t^2} + \bar{\kappa}[2(\varepsilon_1+\varepsilon_2)\frac{\partial J_3}{\partial x} - 4\varepsilon_1\varepsilon_2\frac{\partial^3 J_3}{\partial x^3}]\frac{\partial^4 w}{\partial x^2\,\partial t^2} + \\
&\bar{\kappa}[(\varepsilon_1+\varepsilon_2)J_3 - 6\varepsilon_1\varepsilon_2\frac{\partial^2 J_3}{\partial x^2}]\frac{\partial^5 w}{\partial x^3\,\partial t^2} + [-4\varepsilon_1\varepsilon_2\bar{\kappa}\frac{\partial J_3}{\partial x}]\frac{\partial^6 w}{\partial x^4\,\partial t^2} + [-\varepsilon_1\varepsilon_2\bar{\kappa}J_3]\frac{\partial^7 w}{\partial x^5\,\partial t^2} = 0
\end{aligned} \tag{22}$$

where

$$\bar{\kappa} = \frac{-4}{3h^2} \tag{23}$$

$$(-\varepsilon_2\alpha_{11} - 2\varepsilon_1\bar{\alpha}_{11})\frac{\partial^4 u}{\partial x^4} + (-2\varepsilon_2\frac{\partial \alpha_{11}}{\partial x} - 4\varepsilon_1\frac{\partial \bar{\alpha}_{11}}{\partial x})\frac{\partial^3 u}{\partial x^3} + (\alpha_{11} + 2\bar{\alpha}_{11} - \varepsilon_2\frac{\partial^2 \alpha_{11}}{\partial x^2} - 2\varepsilon_1\frac{\partial^2 \bar{\alpha}_{11}}{\partial x^2})\frac{\partial^2 u}{\partial x^2} +$$
$$(-\varepsilon_2\zeta_{11} - 2\varepsilon_1\bar{\zeta}_{11})\frac{\partial^4 \psi}{\partial x^4} + (-2\varepsilon_2\frac{\partial \zeta_{11}}{\partial x} - 4\varepsilon_1\frac{\partial \bar{\zeta}_{11}}{\partial x})\frac{\partial^3 \psi}{\partial x^3} + (\zeta_{11} + 2\bar{\zeta}_{11} - \varepsilon_2\frac{\partial^2 \zeta_{11}}{\partial x^2} - 2\varepsilon_1\frac{\partial^2 \bar{\zeta}_{11}}{\partial x^2} + 2\varepsilon_1\bar{A})\frac{\partial^2 \psi}{\partial x^2} +$$
$$(4\varepsilon_1\frac{\partial \bar{A}}{\partial x})\frac{\partial \psi}{\partial x} + (-2\bar{A} + 2\varepsilon_1\frac{\partial^2 \bar{A}}{\partial x^2})\psi + \bar{\kappa}(-\varepsilon_2\delta_{11} - 2\varepsilon_1\bar{\delta}_{11})\frac{\partial^5 w}{\partial x^5} + \bar{\kappa}(-2\varepsilon_2\frac{\partial \delta_{11}}{\partial x} - 4\varepsilon_1\frac{\partial \bar{\delta}_{11}}{\partial x})\frac{\partial^4 w}{\partial x^4}$$
$$[\bar{\kappa}(\delta_{11} + 2\bar{\delta}_{11} - \varepsilon_2\frac{\partial^2 \delta_{11}}{\partial x^2} - 2\varepsilon_1\frac{\partial^2 \bar{\delta}_{11}}{\partial x^2}) + 2\varepsilon_1\bar{A}]\frac{\partial^3 w}{\partial x^3} + (4\varepsilon_1\frac{\partial \bar{A}}{\partial x})\frac{\partial^2 w}{\partial x^2} + (-2\bar{A} + 2\varepsilon_1\frac{\partial^2 \bar{A}}{\partial x^2})\frac{\partial w}{\partial x} +$$
$$[-\hat{J}_1 + (\varepsilon_1 + \varepsilon_2)\frac{\partial^2 \hat{J}_1}{\partial x^2} - \varepsilon_1\varepsilon_2\frac{\partial^4 \hat{J}_1}{\partial x^4}]\frac{\partial^2 u}{\partial t^2} + [2(\varepsilon_1 + \varepsilon_2)\frac{\partial \hat{J}_1}{\partial x} - 4\varepsilon_1\varepsilon_2\frac{\partial^3 \hat{J}_1}{\partial x^3}]\frac{\partial^3 u}{\partial x\,\partial t^2} +$$
$$[(\varepsilon_1 + \varepsilon_2)\hat{J}_1 - 6\varepsilon_1\varepsilon_2\frac{\partial^2 \hat{J}_1}{\partial x^2}]\frac{\partial^4 u}{\partial x^2\,\partial t^2} + [-4\varepsilon_1\varepsilon_2\frac{\partial \hat{J}_1}{\partial x}]\frac{\partial^5 u}{\partial x^3\,\partial t^2} + [-\varepsilon_1\varepsilon_2\hat{J}_1]\frac{\partial^6 u}{\partial x^4\,\partial t^2} +$$
$$[-\bar{J}_2 + (\varepsilon_1 + \varepsilon_2)\frac{\partial^2 \bar{J}_2}{\partial x^2} - \varepsilon_1\varepsilon_2\frac{\partial^4 \bar{J}_2}{\partial x^4}]\frac{\partial^2 \psi}{\partial t^2} + [2(\varepsilon_1 + \varepsilon_2)\frac{\partial \bar{J}_2}{\partial x} - 4\varepsilon_1\varepsilon_2\frac{\partial^3 \bar{J}_2}{\partial x^3}]\frac{\partial^3 \psi}{\partial x\,\partial t^2} +$$
$$[(\varepsilon_1 + \varepsilon_2)\bar{J}_2 - 6\varepsilon_1\varepsilon_2\frac{\partial^2 \bar{J}_2}{\partial x^2}]\frac{\partial^4 \psi}{\partial x^2\,\partial t^2} + [-4\varepsilon_1\varepsilon_2\frac{\partial \bar{J}_2}{\partial x}]\frac{\partial^5 \psi}{\partial x^3\,\partial t^2} + [-\varepsilon_1\varepsilon_2\bar{J}_2]\frac{\partial^6 \psi}{\partial x^4\,\partial t^2} +$$
$$\bar{\kappa}[-\hat{J}_4 + (\varepsilon_1 + \varepsilon_2)\frac{\partial^2 \hat{J}_4}{\partial x^2} - \varepsilon_1\varepsilon_2\frac{\partial^4 \hat{J}_4}{\partial x^4}]\frac{\partial^3 w}{\partial x\,\partial t^2} + \bar{\kappa}[2(\varepsilon_1 + \varepsilon_2)\frac{\partial \hat{J}_4}{\partial x} - 4\varepsilon_1\varepsilon_2\frac{\partial^3 \hat{J}_4}{\partial x^3}]\frac{\partial^4 w}{\partial x^2\,\partial t^2} +$$
$$\bar{\kappa}[(\varepsilon_1 + \varepsilon_2)\hat{J}_4 - 6\varepsilon_1\varepsilon_2\frac{\partial^2 \hat{J}_4}{\partial x^2}]\frac{\partial^5 w}{\partial x^3\,\partial t^2} + [-4\varepsilon_1\varepsilon_2\bar{\kappa}\frac{\partial \hat{J}_4}{\partial x}]\frac{\partial^6 w}{\partial x^4\,\partial t^2} + [-\varepsilon_1\varepsilon_2\bar{\kappa}\hat{J}_4]\frac{\partial^7 w}{\partial x^5\,\partial t^2} = 0$$

(24)

and where

$$\zeta_{11} = \beta_{11} + \bar{\kappa}\delta_{11}$$
$$\bar{\zeta}_{11} = \bar{\beta}_{11} + \bar{\kappa}\bar{\delta}_{11} \tag{25}$$
$$\bar{J}_2 = \hat{J}_2 + \bar{\kappa}\hat{J}_4$$

$$\bar{\kappa}(\varepsilon_2 E_{11}+2\varepsilon_1\bar{E}_{11})\frac{\partial^5 u}{\partial x^5}+\bar{\kappa}(2\varepsilon_2\frac{\partial E_{11}}{\partial x}+4\varepsilon_1\frac{\partial \bar{E}_{11}}{\partial x})\frac{\partial^4 u}{\partial x^4}+\bar{\kappa}(-E_{11}-2\bar{E}_{11}+\varepsilon_2\frac{\partial^2 E_{11}}{\partial x^2}+2\varepsilon_1\frac{\partial^2 \bar{E}_{11}}{\partial x^2})\frac{\partial^3 u}{\partial x^3}+$$
$$\bar{\kappa}(\varepsilon_2\delta_{11}+2\varepsilon_1\bar{\delta}_{11})\frac{\partial^5 \psi}{\partial x^5}+\bar{\kappa}(2\varepsilon_2\frac{\partial \delta_{11}}{\partial x}+4\varepsilon_1\frac{\partial \bar{\delta}_{11}}{\partial x})\frac{\partial^4 \psi}{\partial x^4}+[-\bar{\kappa}(\delta_{11}+2\bar{\delta}_{11}+\varepsilon_2\frac{\partial^2 \delta_{11}}{\partial x^2}+2\varepsilon_1\frac{\partial^2 \bar{\delta}_{11}}{\partial x^2})-2\varepsilon_1\bar{A}]\frac{\partial^3 \psi}{\partial x^3}+$$
$$(-4\varepsilon_1\frac{\partial \bar{A}}{\partial x})\frac{\partial^2 \psi}{\partial x^2}+(2\bar{A}-2\varepsilon_1\frac{\partial^2 \bar{A}}{\partial x^2})\frac{\partial \psi}{\partial x}+[\bar{\kappa}^2(\varepsilon_2 H_{11}+2\varepsilon_1\bar{H}_{11})+\varepsilon_1\varepsilon_2 T]\frac{\partial^6 w}{\partial x^6}+[\bar{\kappa}^2(2\varepsilon_2\frac{\partial H_{11}}{\partial x}+4\varepsilon_1\frac{\partial \bar{H}_{11}}{\partial x})+$$
$$5\varepsilon_1\varepsilon_2\frac{\partial T}{\partial x}]\frac{\partial^5 w}{\partial x^5}+[-\bar{\kappa}^2(H_{11}+2\bar{H}_{11}+\varepsilon_2\frac{\partial^2 H_{11}}{\partial x^2}+2\varepsilon_1\frac{\partial^2 \bar{H}_{11}}{\partial x^2})-2\varepsilon_1\bar{A}-(\varepsilon_1+\varepsilon_2)T+10\varepsilon_1\varepsilon_2\frac{\partial^2 T}{\partial x^2}]\frac{\partial^4 w}{\partial x^4}+$$
$$[-4\varepsilon_1\frac{\partial \bar{A}}{\partial x}-3(\varepsilon_1+\varepsilon_2)\frac{\partial T}{\partial x}]\frac{\partial^3 w}{\partial x^3}+[2\bar{A}-2\varepsilon_1\frac{\partial^2 \bar{A}}{\partial x^2}+T-3(\varepsilon_1+\varepsilon_2)\frac{\partial^2 T}{\partial x^2}]\frac{\partial^2 w}{\partial x^2}+(\frac{\partial T}{\partial x})\frac{\partial w}{\partial x}+$$
$$\bar{\kappa}[+J_3-(\varepsilon_1+\varepsilon_2)\frac{\partial^2 J_3}{\partial x^2}+\varepsilon_1\varepsilon_2\frac{\partial^4 J_3}{\partial x^4}]\frac{\partial^3 u}{\partial x\,\partial t^2}+\bar{\kappa}[-2(\varepsilon_1+\varepsilon_2)\frac{\partial J_3}{\partial x}+4\varepsilon_1\varepsilon_2\frac{\partial^3 J_3}{\partial x^3}]\frac{\partial^4 u}{\partial x^2\,\partial t^2}+$$
$$\bar{\kappa}[-(\varepsilon_1+\varepsilon_2)J_3+6\varepsilon_1\varepsilon_2\frac{\partial^2 J_3}{\partial x^2}]\frac{\partial^5 u}{\partial x^3\,\partial t^2}+[4\varepsilon_1\varepsilon_2\bar{\kappa}\frac{\partial J_3}{\partial x}]\frac{\partial^6 u}{\partial x^4\,\partial t^2}+[\varepsilon_1\varepsilon_2\bar{\kappa}J_3]\frac{\partial^7 u}{\partial x^5\,\partial t^2}+$$
$$\bar{\kappa}[+\hat{J}_4-(\varepsilon_1+\varepsilon_2)\frac{\partial^2 \hat{J}_4}{\partial x^2}+\varepsilon_1\varepsilon_2\frac{\partial^4 \hat{J}_4}{\partial x^4}]\frac{\partial^3 \psi}{\partial x\,\partial t^2}+\bar{\kappa}[-2(\varepsilon_1+\varepsilon_2)\frac{\partial \hat{J}_4}{\partial x}+4\varepsilon_1\varepsilon_2\frac{\partial^3 \hat{J}_4}{\partial x^3}]\frac{\partial^4 \psi}{\partial x^2\,\partial t^2}+$$
$$\bar{\kappa}[-(\varepsilon_1+\varepsilon_2)\hat{J}_4+6\varepsilon_1\varepsilon_2\frac{\partial^2 \hat{J}_4}{\partial x^2}]\frac{\partial^5 \psi}{\partial x^3\,\partial t^2}+[4\varepsilon_1\varepsilon_2\bar{\kappa}\frac{\partial \hat{J}_4}{\partial x}]\frac{\partial^6 \psi}{\partial x^4\,\partial t^2}+[\varepsilon_1\varepsilon_2\bar{\kappa}\hat{J}_4]\frac{\partial^7 \psi}{\partial x^5\,\partial t^2}$$
$$[-J_0+(\varepsilon_1+\varepsilon_2)\frac{\partial^2 J_0}{\partial x^2}-\varepsilon_1\varepsilon_2\frac{\partial^4 J_0}{\partial x^4}]\frac{\partial^2 w}{\partial t^2}+[2(\varepsilon_1+\varepsilon_2)\frac{\partial J_0}{\partial x}-4\varepsilon_1\varepsilon_2\frac{\partial^3 J_0}{\partial x^3}]\frac{\partial^3 w}{\partial x\,\partial t^2}+$$
$$[\bar{\kappa}^2 J_6+(\varepsilon_1+\varepsilon_2)J_0-\bar{\kappa}^2(\varepsilon_1+\varepsilon_2)\frac{\partial^2 J_6}{\partial x^2}-6\varepsilon_1\varepsilon_2\frac{\partial^2 J_0}{\partial x^2}+\varepsilon_1\varepsilon_2\bar{\kappa}^2\frac{\partial^4 J_6}{\partial x^4}]\frac{\partial^4 w}{\partial x^2\,\partial t^2}+$$
$$[-2\bar{\kappa}^2(\varepsilon_1+\varepsilon_2)\frac{\partial J_6}{\partial x}-4\varepsilon_1\varepsilon_2\frac{\partial J_0}{\partial x}+4\varepsilon_1\varepsilon_2\bar{\kappa}^2\frac{\partial^3 J_6}{\partial x^3}]\frac{\partial^5 w}{\partial x^3\,\partial t^2}+$$
$$[-\bar{\kappa}^2(\varepsilon_1+\varepsilon_2)J_6-\varepsilon_1\varepsilon_2 J_0+6\varepsilon_1\varepsilon_2\bar{\kappa}^2\frac{\partial^2 J_6}{\partial x^2}]\frac{\partial^6 w}{\partial x^4\,\partial t^2}+[4\varepsilon_1\varepsilon_2\bar{\kappa}^2\frac{\partial J_6}{\partial x}]\frac{\partial^7 w}{\partial x^5\,\partial t^2}+[\varepsilon_1\varepsilon_2\bar{\kappa}^2 J_6]\frac{\partial^8 w}{\partial x^6\,\partial t^2}=0 \tag{26}$$

3. Solution Procedure

The analytical solution of governing equations for wave propagation in the 2D-FG nano-beam is established in this section. Using the harmonic method, the displacement fields for the wave propagation is defined as:

$$\begin{Bmatrix} u(x,t) \\ \psi(x,t) \\ w(x,t) \end{Bmatrix} = \begin{Bmatrix} u_0 \exp[i(Kx-\omega t)] \\ \psi_0 \exp[i(Kx-\omega t)] \\ w_0 \exp[i(Kx-\omega t)] \end{Bmatrix} \tag{27}$$

where, K and ω indicate the wave number and circular frequency, respectively. (u_0, ψ_0, w_0) are the wave amplitudes and $i=\sqrt{-1}$. Because the present study considers wave propagation in unbounded elastic domains, it is not necessary to consider the boundary conditions [22, 49-53].

By inserting Eq. (27) and its derivatives into Eqs. (22), (24) and (26), the characteristic equation is extracted as:

$$(\mathbf{K}-\omega^2\mathbf{M})\mathbf{X}=0 \tag{28}$$

where $\mathbf{X}=(u_0,\psi_0,w_0)$ is the eigenvector. $\mathbf{M}$ and $\mathbf{K}$ are the mass and stiffness matrices, respectively, and include complex terms. Also, the phase velocity of waves can be easily computed by $c=\omega/K$.

It should be noted that the material properties change along beam, and here the Chebyshev–Gauss–Lobatto distribution is employed to discretize the length of the nano-beam, as

$$x_N=\frac{1}{2}\left(1-\cos(\frac{N-1}{\Gamma-1})\pi\right) \qquad N=1,2,...,\Gamma \tag{29}$$

where x_N is the x coordinate of the N^{th} node along the nano-beam. $\Gamma=27$ is the number of discrete nodes assumed along the x direction of the nano-beam (see Fig. 2). It should be noted that this discretization is only used to specify the material properties; the choice of Γ only depends on material distribution, and does not affect the numerical convergence of the results. Hence Eq. (28) is used to calculate the eigenvalues at only one point with its specific mechanical properties. The modelled nano-beam is assumed to have a square cross section $(h=b)$.

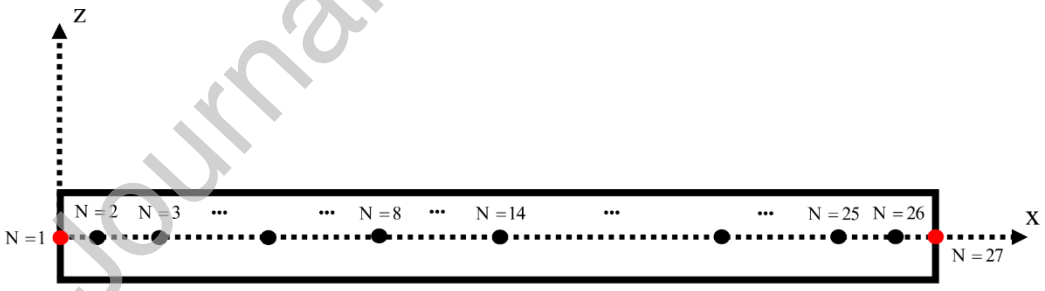

Fig. 2. Domain discretization by the Chebyshev–Gauss–Lobatto distribution along the nano-beam

4. Numerical Results and Discussions

In this section, the numerical results are extracted and discussed for the wave propagation of the rotating 2D-FG nano-beam by considering the variation of five parameters, namely $nx, nz, \gamma, \Omega, L/h$. Also, the effects of the power law indexes, nx, nz, the porosity volume fraction γ, the dimensionless beam rotating velocity Ω and the ratio of length to thickness of the nano-beam, L/h, are shown. For this purpose, we fix four out of the five parameters at each step, and change the remaining parameter to investigate the effects. The material properties of the 2D nano-beam are given in Table 1.

Table 1: Material properties of the FGM [47]

Material	$\lambda(GPa)$	$\mu(GPa)$	$\varepsilon_1(nm^2)$	$\varepsilon_1(nm^2)$	$a(nm)$	$\rho(kg/m^3)$
Copper (Cu)	25	78	$0.17a^2$	$0.03a^2$	0.3597	8960
Barium Oxide (BaO)	48.1	38.8	$0.15a^2$	$0.045a^2$	0.5537	5720

4.1. Model Validation

To validate the present model and to verify of the accuracy of results, the numerical results from the present model with the materials of Ref. [54] are compared with the results in Ref. [54]. Thus, we reduced our 2D-FG model to a 1D-FG nano-beam by setting $nx = 0$. Also, by assuming $\sqrt{\varepsilon_1} = \sqrt{\varepsilon_2} = \mu$, the GNT is reduced to Eringen's nonlocal theory which was used in Ref. [54]. Table 2 gives the results for various values of nonlocal parameter μ. The comparison of the results in Table 2 shows a good agreement between the results of the present method and the results of Ref. [54] and verifies the accuracy of our model.

Table 2: Comparison of the frequency for FG nano-beam $n_z = 1;\ \Omega = 1(Grad/s)$

$\sqrt{\varepsilon_1} = \sqrt{\varepsilon_2} = \mu$	$K = 1\ (nm)^{-1}$		$K = 10\ (nm)^{-1}$	
	Ref. [54]	**Present**	**Ref. [54]**	**Present**
1 (nm)	0.5371	0.5304	0.7546	0.7487
2 (nm)	0.4298	0.4253	0.5382	0.5342
3 (nm)	0.3978	0.3951	0.4138	0.4102

4.2. The Effects of n_x and n_z

The effects of the power law indexes, n_x and n_z, on the frequency for the longitudinal (LA), transverse (TA) and torsional (TO) wave propagation are illustrated in Figs. 3, 4 and 5, respectively. Based on the variation of n_x, each of the figures includes 2 different types of graphs. In the first type, which is denoted by the caption (…-1), n_x varies from 0.1 to 1 in 4 steps. In the second type, with caption (…-2), the results are presented for $n_x > 1$, where n_x varies from 1.25 to 2 in 4 steps. On the other hand, for each subfigure the values of n_z is varied from 0 to 5 in 9 steps, denoted by captions (a-…) to (i-…). Therefore, each of Figs. 3, 4 and 5 includes 18 separate graphs. Figures 3, 4 and 5 are plotted for $N = 23$ and $L/h = 100$, $\Omega = 0, \gamma = 0$.

Figure 3 shows the variation of the LA wave frequency versus the wave number. It can be easily observed that the variation of n_x affects the frequency and the variation of n_z affects both the amplitude and the trend of the frequency graphs.

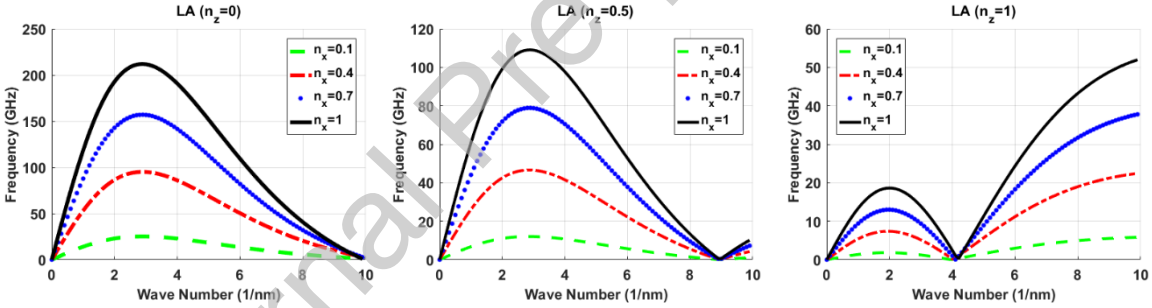

(a-1) (b-1) (c-1)

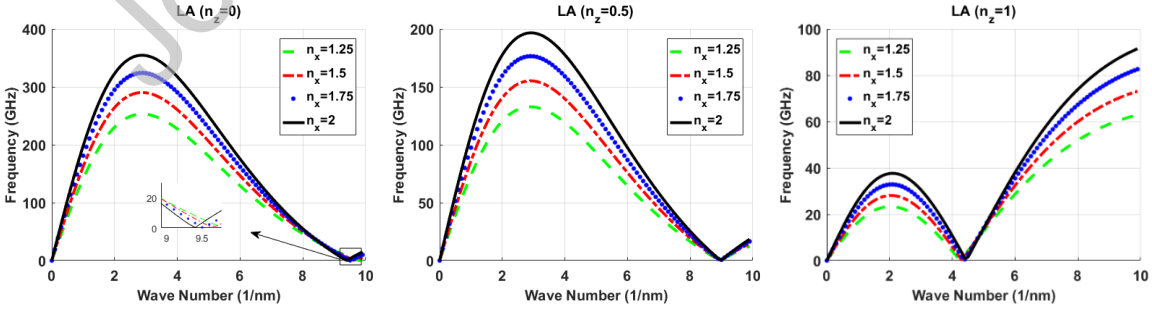

(a-2) (b-2) (c-2)

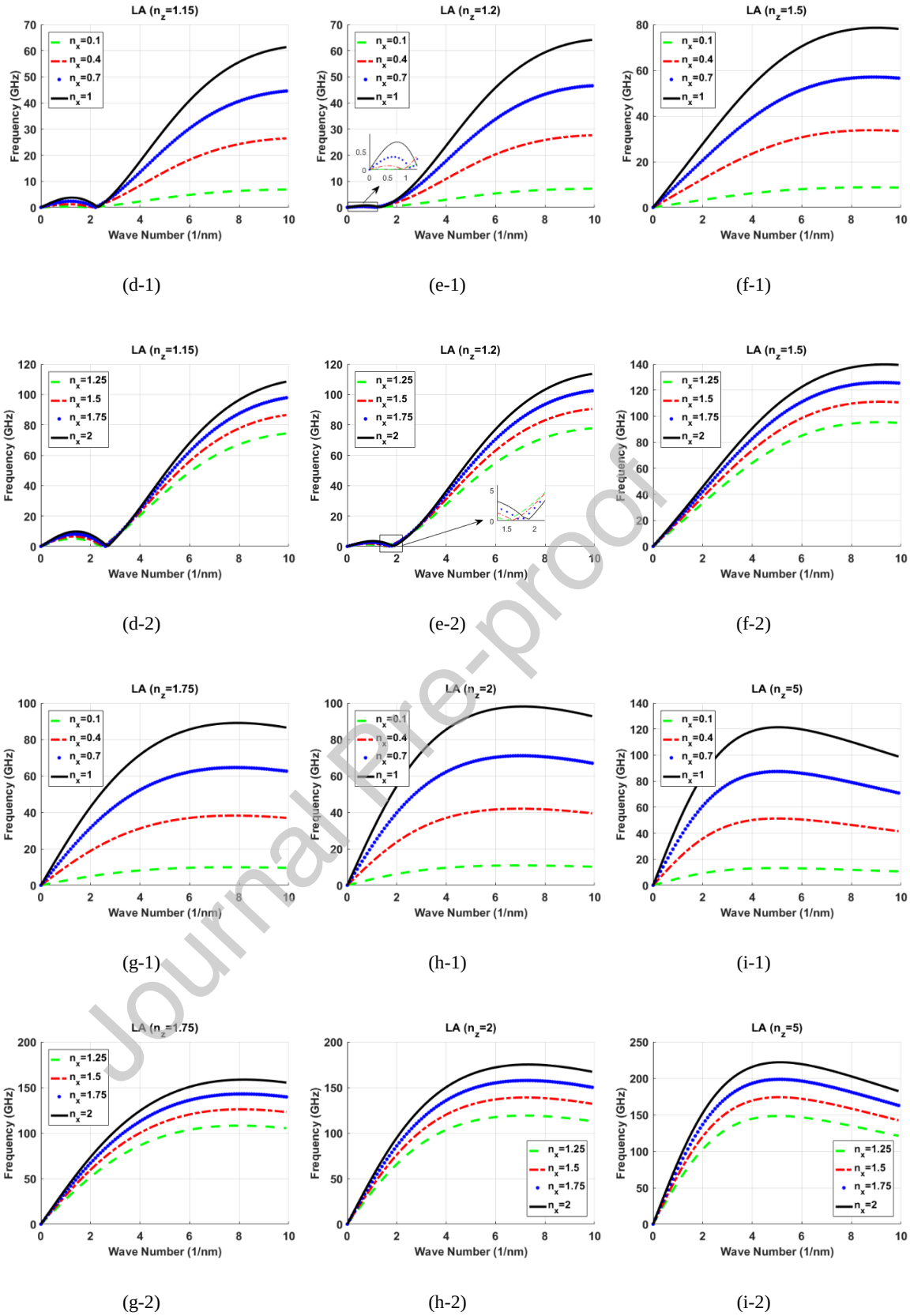

Fig. 3: The effects of n_x and n_z on the longitudinal wave propagation

$(N = 23; L/h = 100; \Omega = 0; \gamma = 0)$

For constant n_z, the LA frequency increases with increasing n_x. However, the effect of the variation of n_z is more complicated. For n_z from 0 to 1.2 the LA frequency graph contains two parts, before and after the convergence point, where the frequency is zero. Increasing n_z from 0 to 1.2 not only moves the convergence point to the left (i.e. a lower wave number) but also decreases the frequency for the wave numbers lower than the convergence point. However, the frequency for wave numbers higher than the convergence point increases with increasing n_z. For values of n_z higher than 1.2, the convergence point vanishes and the frequency increases with increasing n_z.

Figures 4 and 5 show the relation of the TA and TO frequencies versus the wave number (K) for various n_x and n_z. Similar to Fig. 3, the TA and TO frequencies increase with increasing n_x. However, the variation with respect to n_z is opposite for a given value of n_x which is described below.

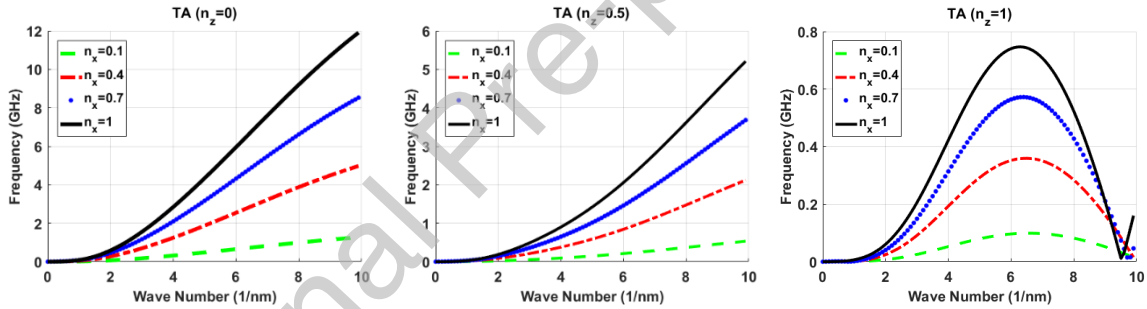

(a-1) (b-1) (c-1)

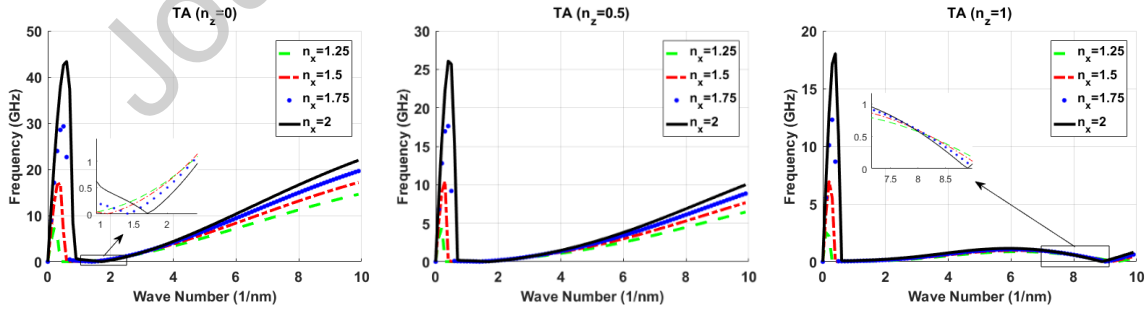

(a-2) (b-2) (c-2)

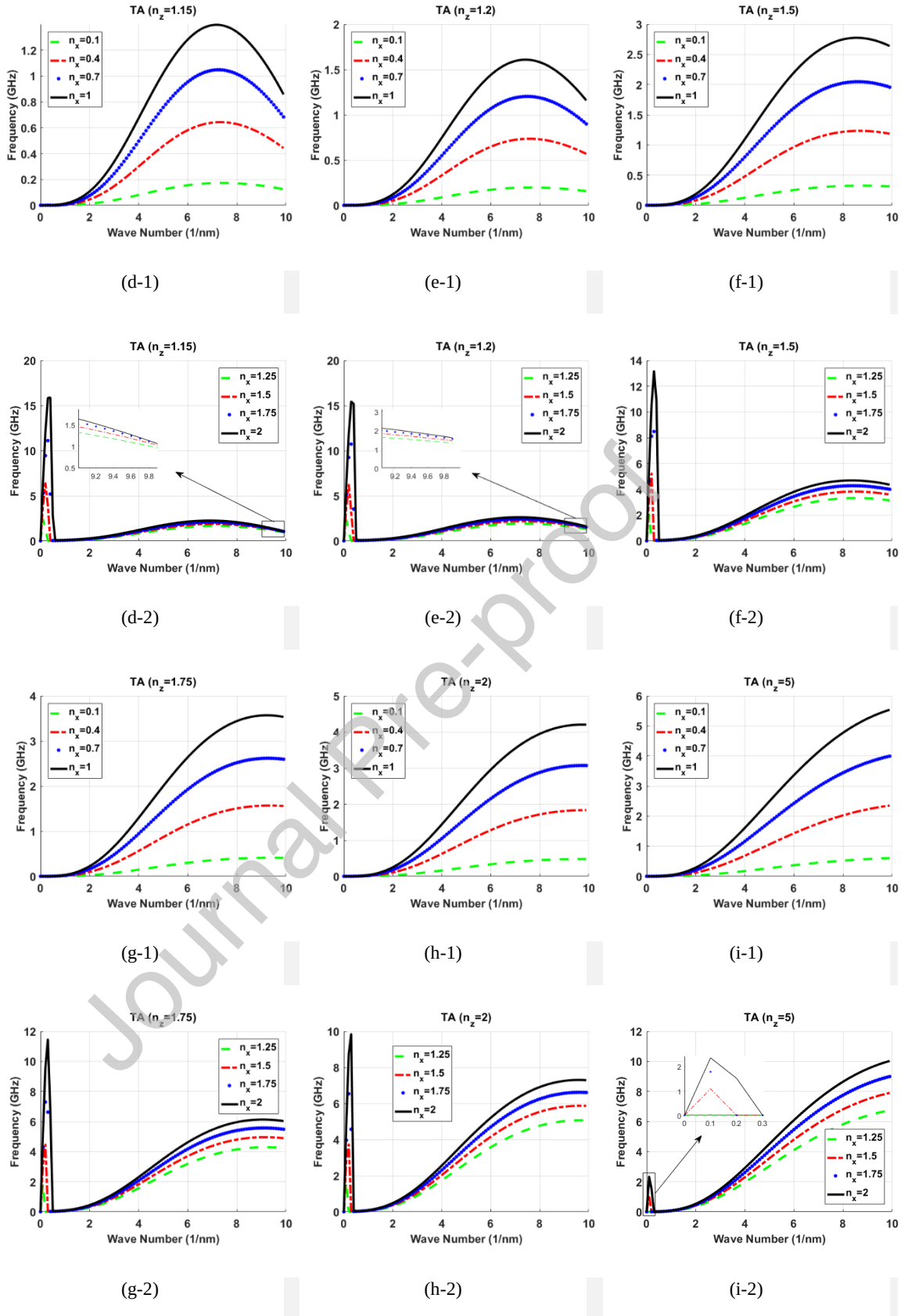

Fig. 4: The effects of n_x and n_z on the transverse wave propagation

$(N = 23; L/h = 100; \Omega = 0; \gamma = 0)$

In Fig. 4, for $n_x \leq 1$ and $n_z < 1$ the frequency increases with increasing wave number. But, for $n_x \leq 1$ and $n_z \geq 1$ the graphs an increasing and then descending trend with increasing wave number from 0 to 10 $(nm)^{-1}$. Although, for some cases, such as Figs. (4)-(h-1) and (4)-(i-1), this trend is not observed for $0 \leq K \leq 10\,(nm)^{-1}$. Also, for $n_x \leq 1$ increasing n_z from 0 to 1 decreases the frequency and increasing n_z above 1 increases the frequency.

On the other hand, in Fig. 4 and for $n_x > 1$ the graphs include 2 parts; before and after the 2nd zero frequency. The second zero frequency can be seen clearly in figures (4)-(a-2) and (4)-(i-2) and occur for $K < 2\,(nm)^{-1}$. Also, increasing n_z decreases the frequency for the first part and increases the frequency for the second part.

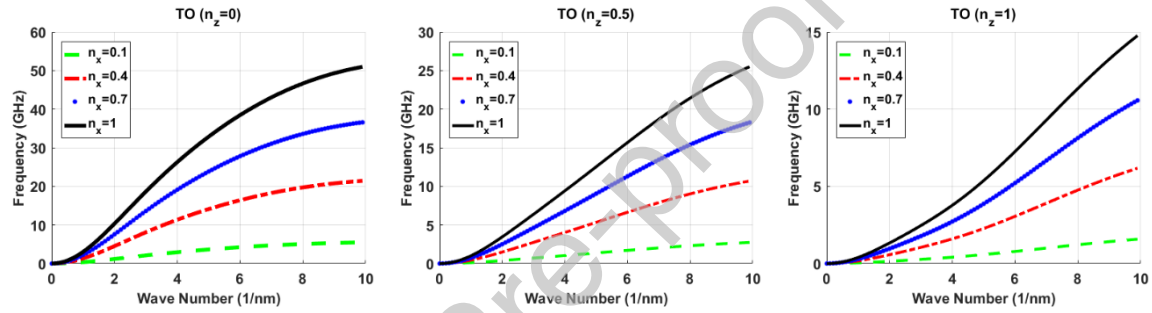

(a-1) (b-1) (c-1)

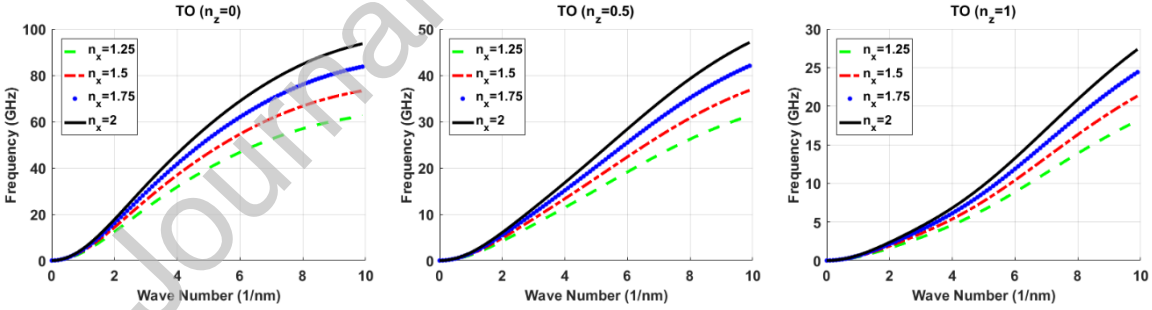

(a-2) (b-2) (c-2)

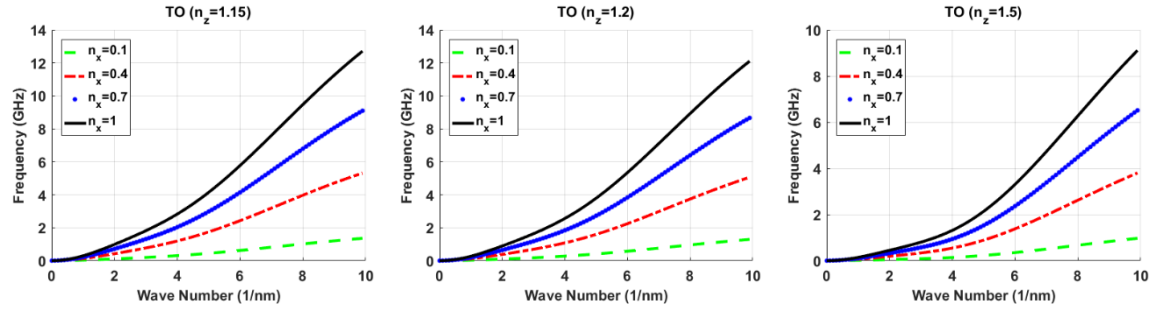

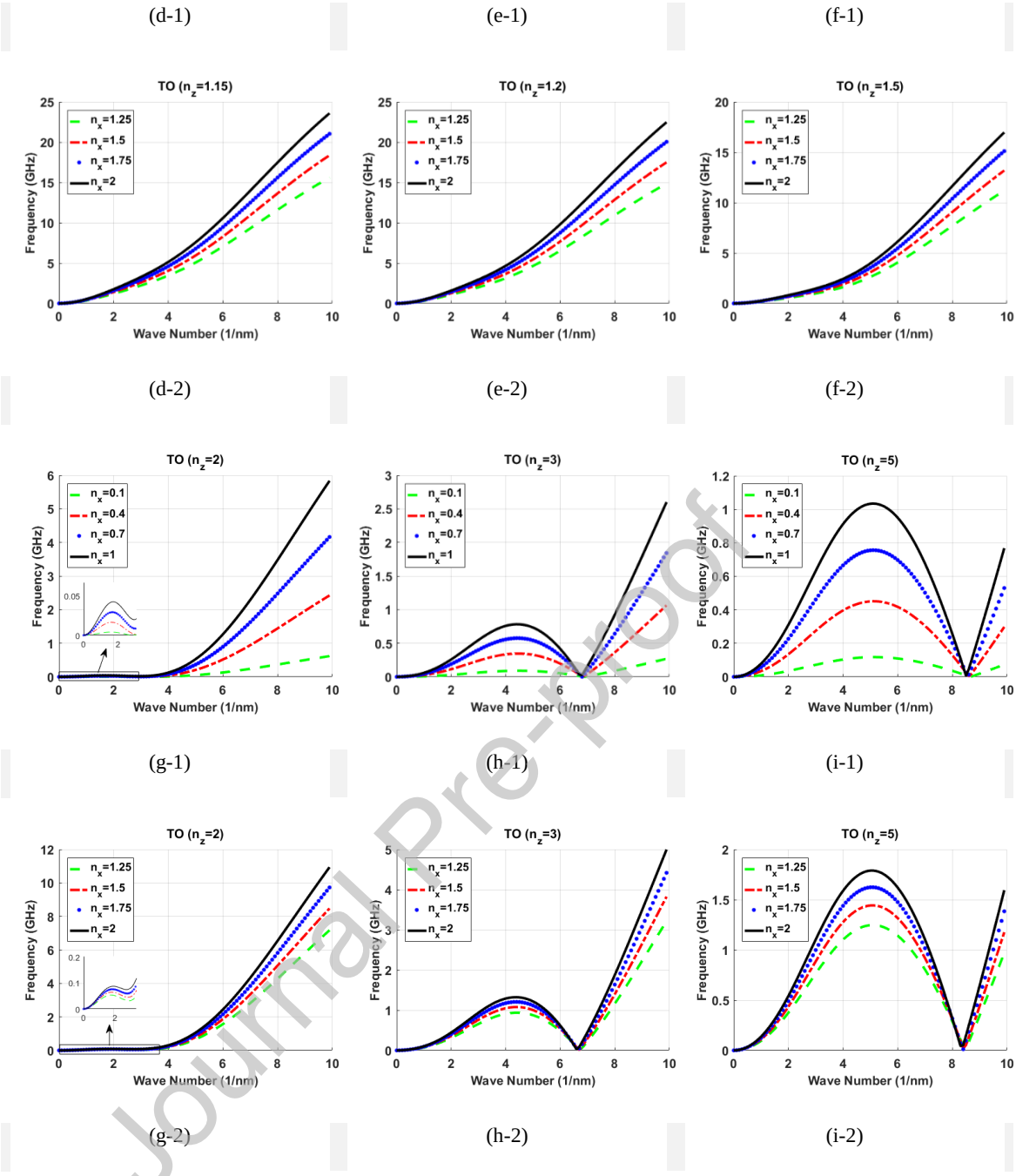

Fig. 5: The effects of n_x and n_z on the torsional wave propagation

$(N = 23; L/h = 100; \Omega = 0; \gamma = 0)$

Figure 5 shows that the TO frequency generally decreases as n_z increases. Also, for all n_x and $n_z < 2$ the trend of graphs is strictly increasing frequency with wave number. But, for $n_z \geq 2$, illustrated in Figs. (5)-(g-1) to (5)-(i-2), the trend of the graphs changes and a local maximum frequency occurs. The value of this maximum increases with increasing n_z above 2.

Clearly from Figs. 3 to 5, the TA, LA and TO frequencies are strongly affected by the variation of n_x and n_z, which motivates their investigation in this current research.

4.3. The Effects of Ω

Figure 6 shows the effects of the dimensionless beam rotating velocity, Ω, on the frequency of TA wave propagation. The dimensionless beam rotating velocity changes from 4 to 16 in 4 steps, and is defined as:

$$\Omega = \tilde{\omega} L^2 \sqrt{\frac{\rho_c A}{E_c I}} \tag{36}$$

where $\tilde{\omega}, L, A, I$ are the rotating velocity, length, area and second moment of area for nano-beam, respectively. Also, ρ_c is the mass density and E_c is the Young's modulus for the pure ceramic part of the FGM.

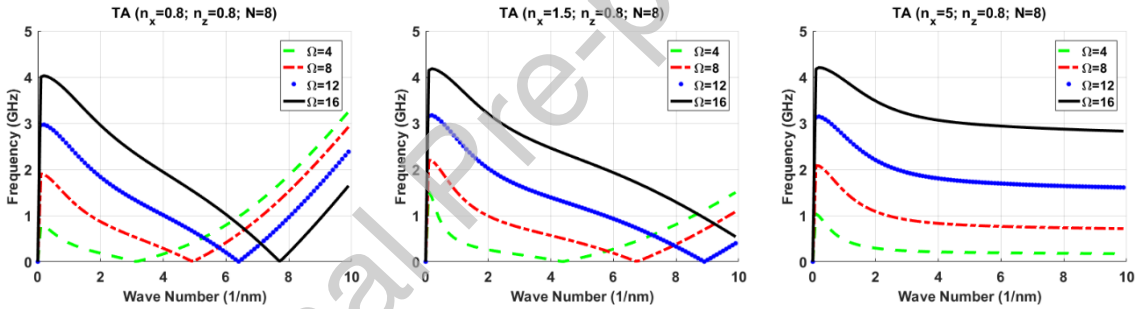

(a-1) (a-2) (a-3)

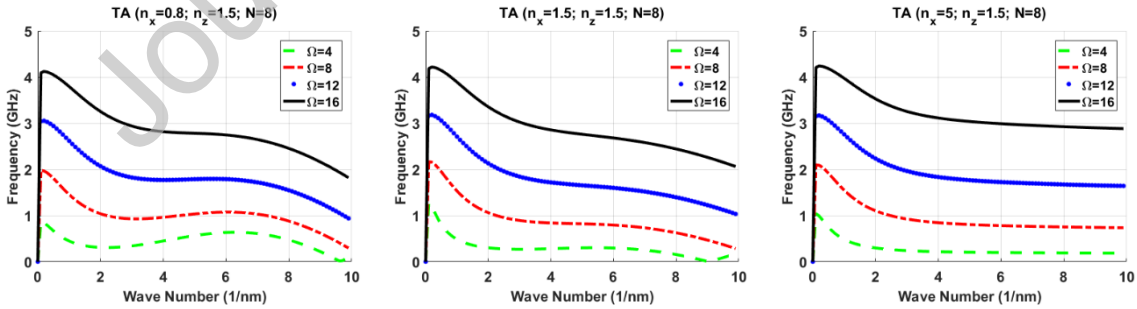

(b-1) (b-2) (b-3)

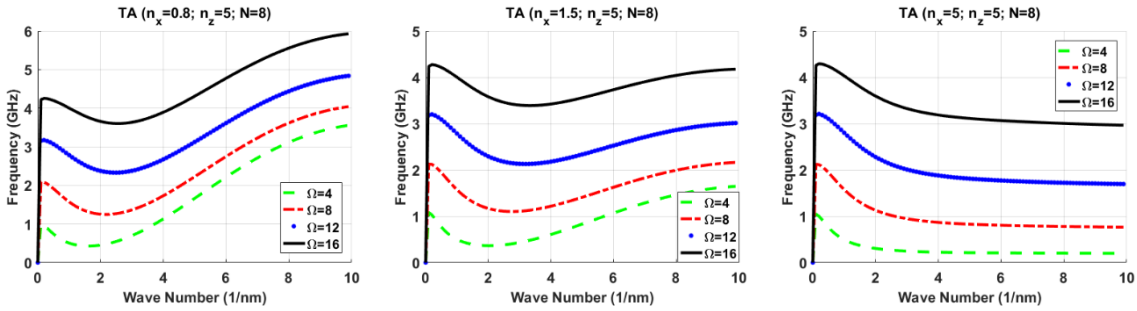

(c-1) (c-2) (c-3)

Fig. 6: The effects of Ω on the transverse wave propagation

$(N = 8; L/h = 100; \gamma = 0)$

Figure 6 is plotted for the 8th node ($N = 8$) on the nano-beam for different values of $n_x, n_z = 0.8, 1.5, 5$. Thus, 9 separate graphs are given. Clearly, increasing the dimensionless beam rotating velocity, increases the TA frequency but the trend of graphs is significantly affected by n_x and n_z. Increasing n_x makes the graphs smoother and increasing n_z increases the frequency for the same wave number.

Figures 7 and 8 show the effects of the dimensionless beam rotating velocity Ω on the frequency of the TO and LA wave propagation, respectively. In Fig. 7 the LA frequency versus wave number is shown for 2 cases, $n_x = n_z = 0.8$ and $n_x = n_z = 5$, and for 3 different nodes, $N = 8, 14, 23$. Clearly, the variation of Ω does not have any significant effect on the frequency of the LA and TO wave propagation.

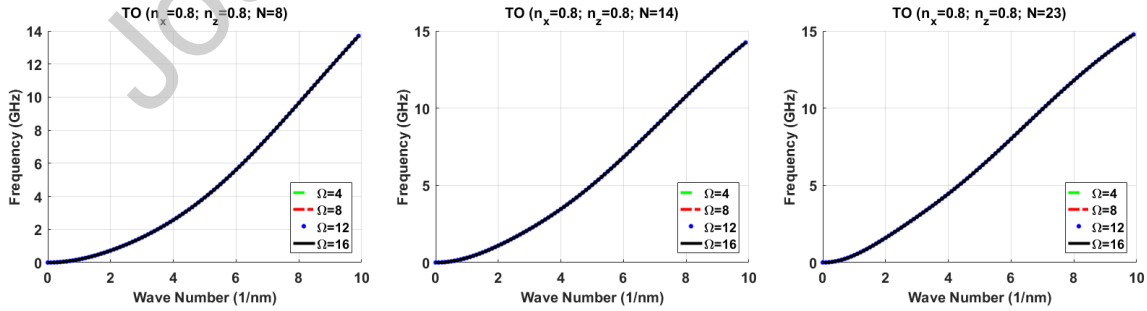

(a-1) (a-2) (a-3)

Fig. 7: The effects of Ω on the torsional wave propagation $(L/h = 100; \gamma = 0)$

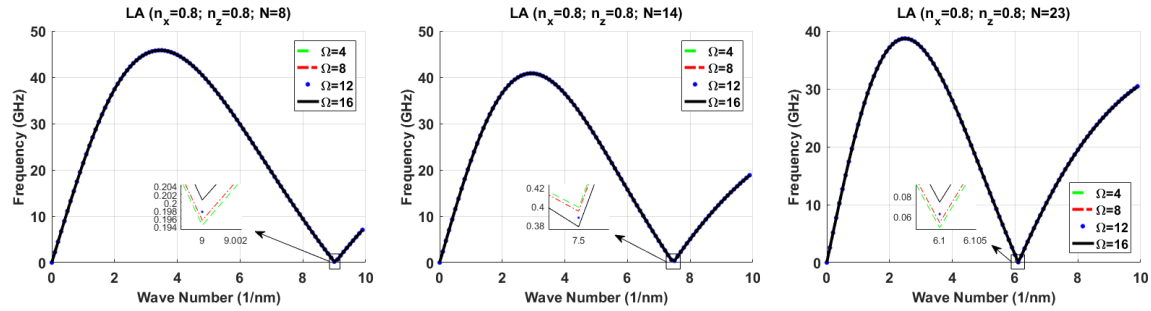

(a-1) (a-2) (a-3)

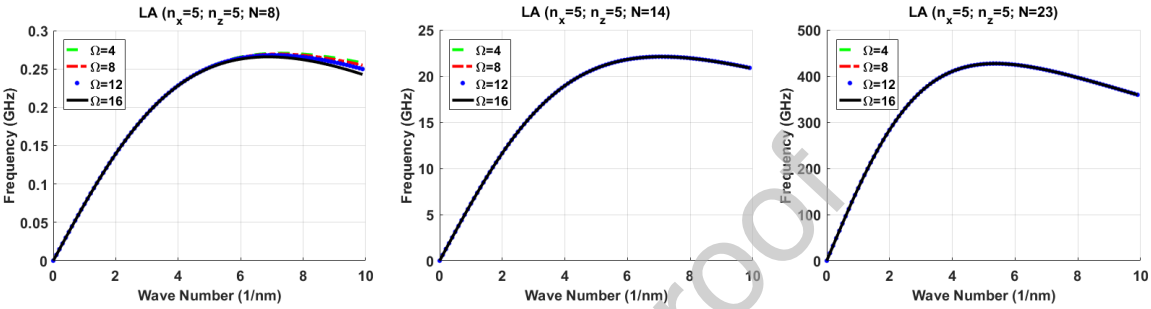

(b-1) (b-2) (b-3)

Fig. 8: The effects of Ω on the longitudinal wave propagation $(L/h=100;\gamma=0)$

4.4. The Effects of γ

Figure 9 shows the effects of the porosity volume fraction γ on the LA, TA an TO frequencies of wave propagation. The graphs are given for $n_x=n_z=1$, $\Omega=0$ and 3 different nodes along the nano-beam ($N=8,14,23$). The changes of γ from 0 to 0.4 has considerable effects on the frequencies for all of the wave propagation types. Although, the quality and intensity of these effects is also associated with the node position along the nano-beam.

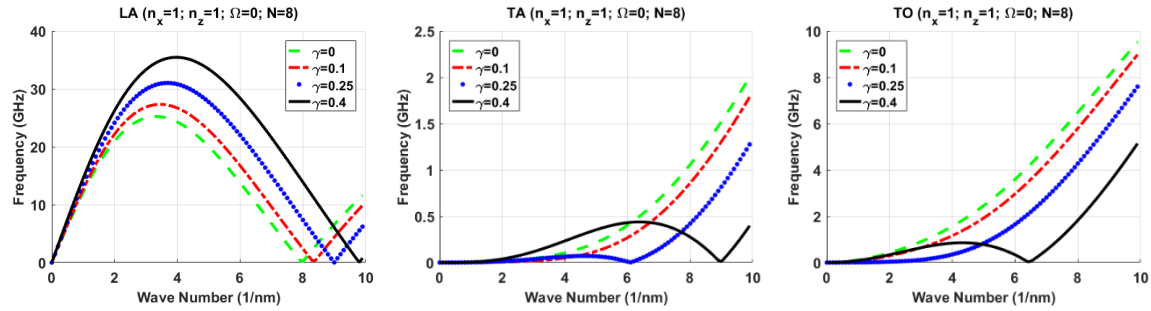

(a-1) (a-2) (a-3)

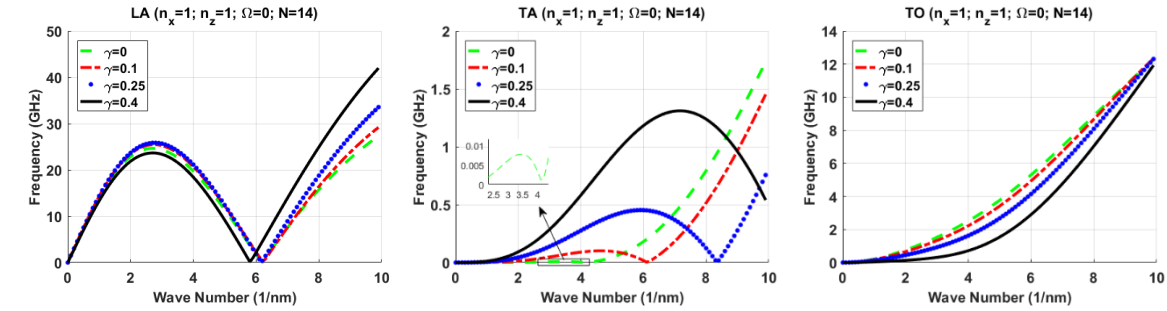

(b-1) (b-2) (b-3)

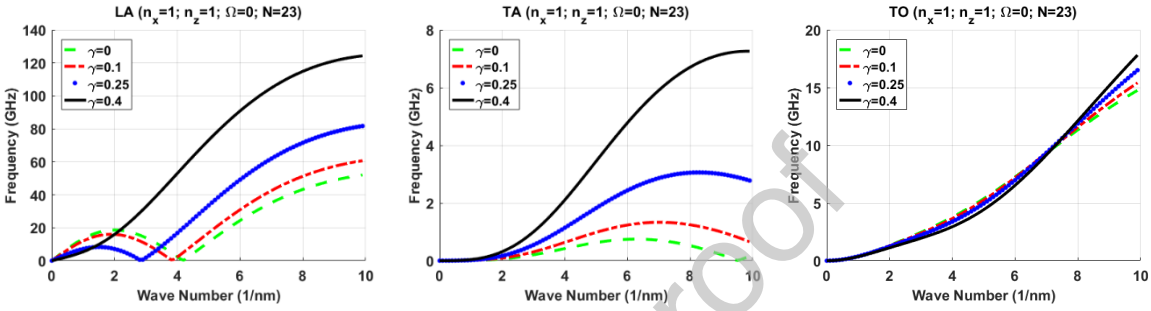

(c-1) (c-2) (c-3)

Fig. 9: The effects of γ on the LA, TA and TO frequencies $(L/h=100)$

4.5. The Effects of L/h

The effects of the ratio of length to thickness for the nano-beam (*L/h*) on the LA, TA and TO frequencies of wave propagation are shown in Fig. 10. The results are plotted for the 14th node with $n_x=n_z=1$, $\Omega=0$ and $\gamma=0$. Considering the results, the variation of the ratio *L/h* has opposite effects on the LA and TA frequencies, and has no significant effect on the TO frequency. Increasing *L/h* increases the LA frequency but decreases the TA frequency. Also, for $L/h<20$ the TO frequency decreases when *L/h* increases for large values of wave number but for $L/h\geq 20$ there are no significant changes.

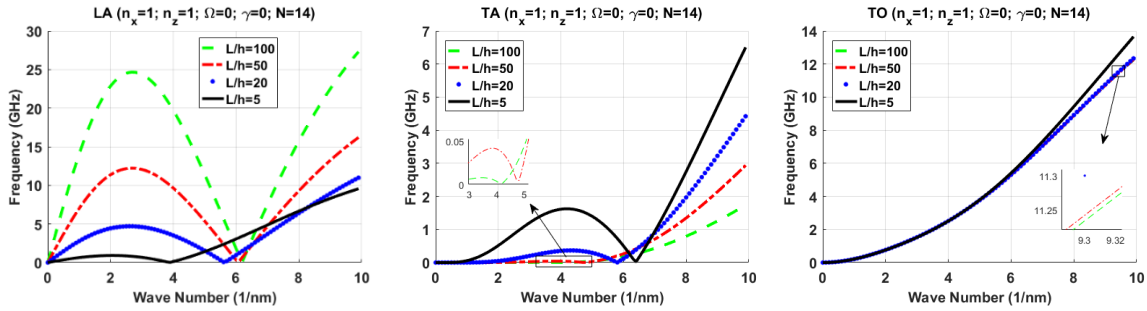

(a-1) (a-2) (a-3)

Fig. 10: The Effects of L/h on the LA, TA and TO frequencies

4.6. Wave Propagation in a 2D Nano-Beam

Figure 11 shows the LA, TA and TO frequencies for wave propagation versus the wave number at 4 different nodes along the nano beam, i.e. the 8th, 14th, 20th and 26th nodes along the nano-beam are selected. The results are extracted for $n_x = 1; n_z = 1.5; \gamma = 0$ and 2 cases of rotational speed, $\Omega = 0$ and $\Omega = 20$. For all situations, the frequencies increase when the number of the node increases. This is confirmed by the results presented in Fig. 12.

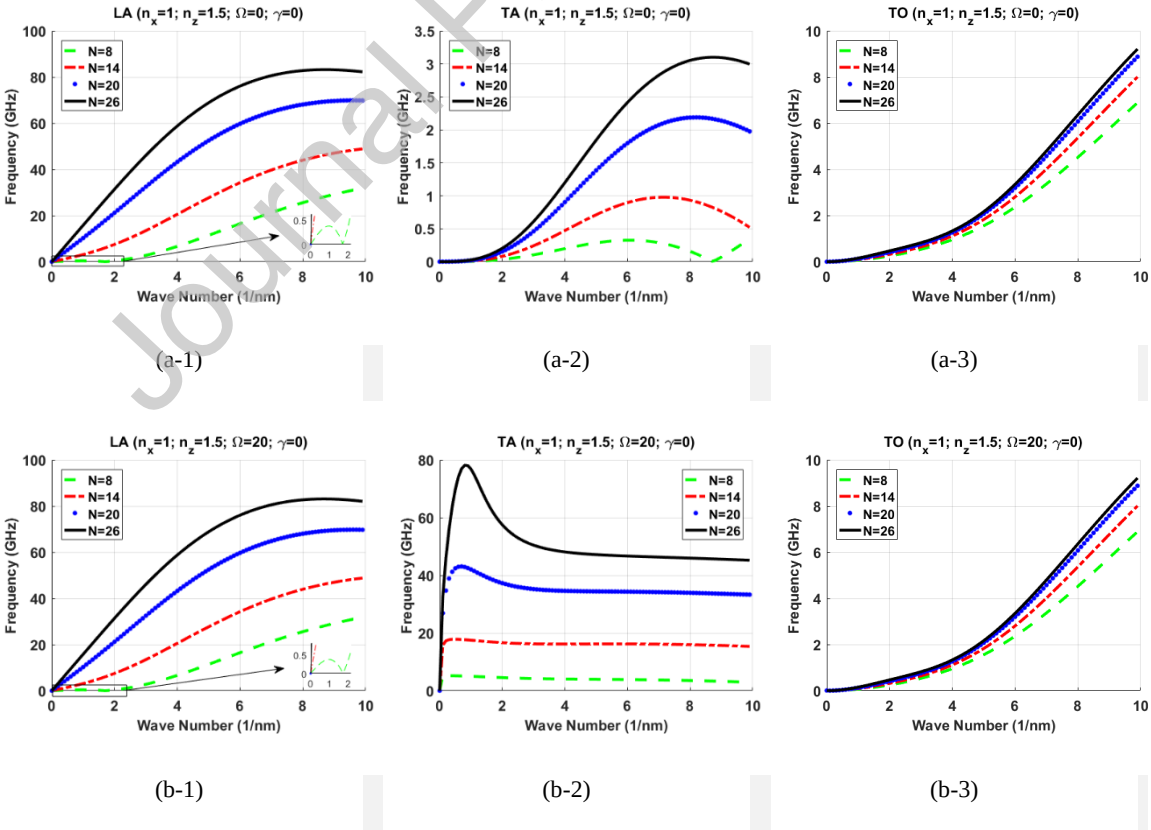

(a-1) (a-2) (a-3)

(b-1) (b-2) (b-3)

Fig. 11: The variation of the LA, TA and TO frequencies at different node locations

The variation of the LA, TA and TO frequencies along the nano-beam is displayed in Fig. 12. The results are plotted for different nodes along the nano-beam from 1 to 27 based on 4 different values of wave number from $K=5(nm)^{-1}$ to $K=10(nm)^{-1}$. Also, the graphs in Fig. 12 are drawn for 3 different values of n_x and n_z, that is $n_x=0.2; n_z=0.5$, $n_x=1; n_z=1.5$ and $n_x=2; n_z=5$. Due to the material property changes along the nano-beam, all types of waves propagation frequencies vary along the nano-beam.

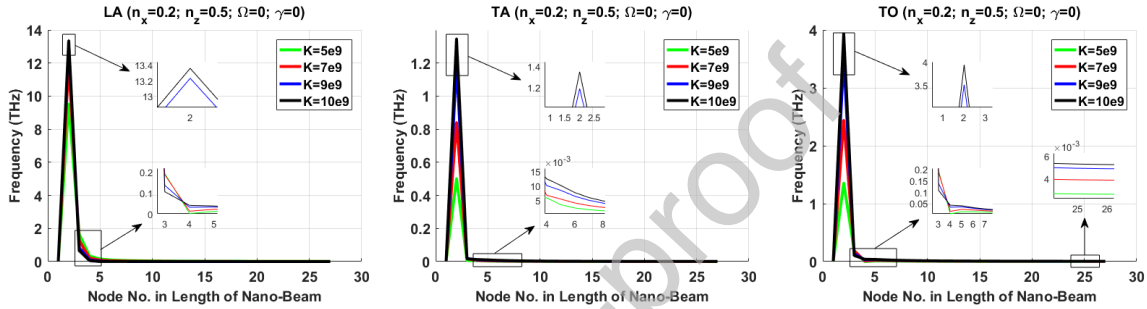

(a-1) (a-2) (a-3)

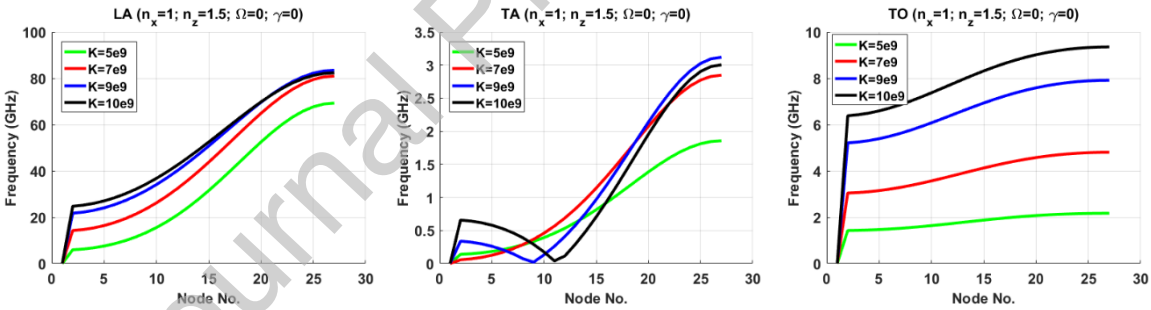

(b-1) (b-2) (b-3)

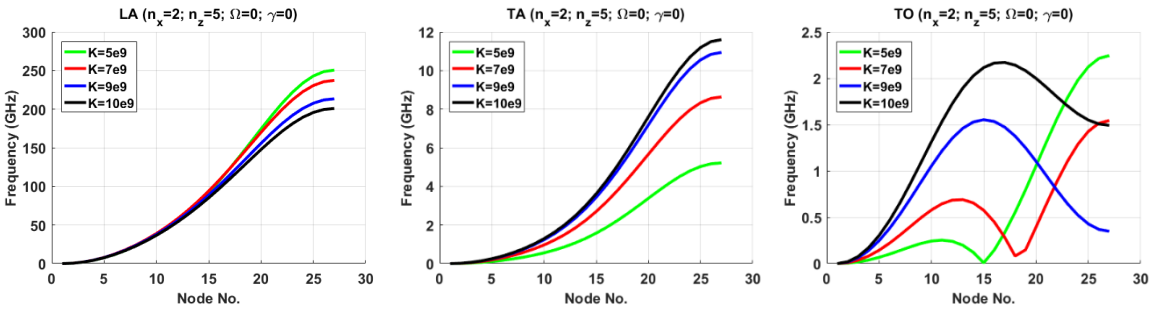

(c-1) (c-2) (c-3)

Fig. 12: The variation of the LA, TA and TO frequencies along the nano-beam for different wave numbers

4.7. The effect of size dependency

Since, in 2D-FG nano beams, the material configuration alters along both the longitudinal and the thickness directions, the nonlocal coefficients ϵ_1 and ϵ_2 also alter along longitudinal (x-axis) and thickness (z-axis) directions, so that

$$\epsilon_1(x,z) = (\epsilon_1)_m + [(\epsilon_1)_c - (\epsilon_1)_m]\left(\frac{1}{2}+\frac{z}{h}\right)^{nz}\left(\frac{x}{L}\right)^{nx} - \frac{\gamma}{2}[(\epsilon_1)_c + (\epsilon_1)_m] \tag{37}$$

$$\epsilon_2(x,z) = (\epsilon_2)_m + [(\epsilon_2)_c - (\epsilon_2)_m]\left(\frac{1}{2}+\frac{z}{h}\right)^{nz}\left(\frac{x}{L}\right)^{nx} - \frac{\gamma}{2}[(\epsilon_2)_c + (\epsilon_2)_m]$$

where the $(\ )_m$ and $(\ )_c$ subscripts denote the metal and ceramic properties respectively.

The effect of size dependency in a pure ceramic is shown by setting $nx = nz = 0$ and employing GNT. Some results are now extracted and discussed.

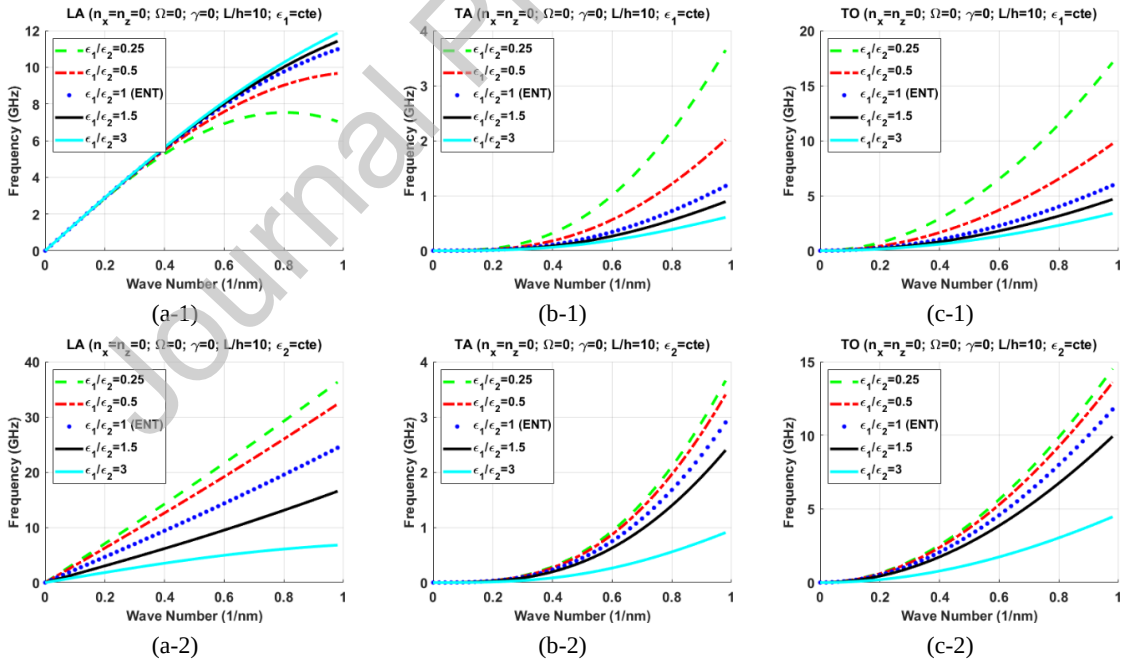

Fig. 13: The effect of constant nonlocal coefficients on the LA, TA and TO frequencies at *L/h*=10

Figure 13 illustrates the effect of the size dependency on predicted frequencies at *L/h*=10. To extract the results in a pure ceramic, we changed the values of ϵ_1 and ϵ_2 in

two different ways. First, we assumed that the value of ϵ_1 was constant and established the results by changing the value of ϵ_2. The results are plotted in Fig. 13 (a-1), (b-1) and (c-1). Then, and for the same ratio of ϵ_1 to ϵ_2, we fixed the value of ϵ_2 and changed the values of ϵ_1 to give the results plotted in Fig. 13 (a-2), (b-2) and (c-2).

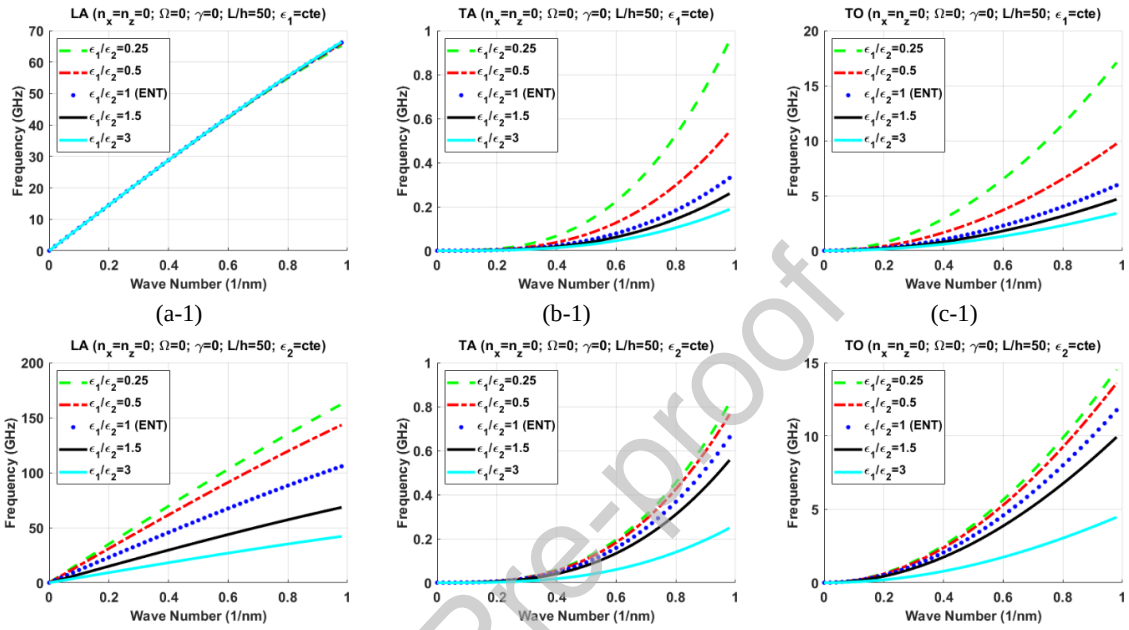

(a-1) (b-1) (c-1)

(a-2) (b-2) (c-2)

Fig. 14: The effect of constant nonlocal coefficients on the LA, TA and TO frequencies at *L/h*=50

Also, the results are reported in Fig. 14 for *L/h*=50. The results show that, except for the LA frequencies with constant ϵ_1 (Figs. 13 (a-1) and 14 (a-1)), the frequencies decrease with an increase in the ratio of ϵ_1 to ϵ_2. In contrast the LA frequencies increase with an increase in ϵ_1/ϵ_2. Although, for high values of *L/h* the variation of ϵ_1/ϵ_2 has no significant effect on the LA frequencies.

It should be noted that for $\epsilon_1 = \epsilon_2$ the GNT reduces to conventional ENT. Hence, employing the conventional ENT to materials with different ϵ_1 and ϵ_2, cannot properly estimate the wave propagation behaviour of materials and this is the main advantage of GNT.

5. Conclusions:

In this research paper, the wave propagation in two dimensional functionally graded rotating nano-beams is studied using a general nonlocal higher-order beam model. To this end, the dispersion relations for each wave mode are derived by solving the three degrees-of-freedom wave characteristic equation of the nano-beam. To illustrate the dispersive nature of the propagating waves, the GNT is used which includes two length-scale parameters in the constitutive equations of the beam. Furthermore, to model the effects of the transverse shear strain on the wave propagation features, the beam is modelled using third-order shear deformation theory. The investigation shows a remarkable phenomenological influence of nonlocal fields in 2D-FG rotating nano-beam on their wave propagation. Thus, the following main conclusions can be derived:

1. The variation of n_x affects the LA frequency and the variation of n_z affects both the amplitude and the trend of LA frequency graphs.

2. The TA and TO frequencies increase with increasing n_x. However, the variation of n_z has the opposite effect on the TA and TO frequencies based on the value of n_x which has been discussed extensively in results section.

3. With increasing dimensionless beam rotating velocity, the TA frequency increases but the trend of graphs is influenced by n_x and n_z. Nevertheless, the variation of the dimensionless beam rotating velocity has no significant effect on the frequency of the LA and TO wave propagation.

4. The change in the porosity significantly affects all types of frequencies for wave propagation. Although, the quality and intensity of these significant effects is associated with the node position along the nano-beam.

5. The variation of the length to thickness ratio has the opposite effect on the LA and TA frequencies. However, it has no significant effect on the TO frequency.

References:

[1] J. Reddy, "Nonlocal theories for bending, buckling and vibration of beams," *International Journal of Engineering Science*, vol. 45, pp. 288-307, 2007.

[2] Q. Wang and K. Liew, "Application of nonlocal continuum mechanics to static analysis of micro-and nano-structures," *Physics Letters A,* vol. 363, pp. 236-242, 2007.

[3] R. Sourki and S. Hosseini, "Coupling effects of nonlocal and modified couple stress theories incorporating surface energy on analytical transverse vibration of a weakened nanobeam," *The European Physical Journal Plus,* vol. 132, p. 184, 2017.

[4] B. Karami, D. Shahsavari, and L. Li, "Temperature-dependent flexural wave propagation in nanoplate-type porous heterogenous material subjected to in-plane magnetic field," *Journal of Thermal Stresses,* vol. 41, pp. 483-499, 2018.

[5] G.-L. She, F.-G. Yuan, and Y.-R. Ren, "On wave propagation of porous nanotubes," *International Journal of Engineering Science,* vol. 130, pp. 62-74, 2018.

[6] L. Lu, X. Guo, and J. Zhao, "Size-dependent vibration analysis of nanobeams based on the nonlocal strain gradient theory," *International Journal of Engineering Science,* vol. 116, pp. 12-24, 2017.

[7] L. Lu, X. Guo, and J. Zhao, "A unified nonlocal strain gradient model for nanobeams and the importance of higher order terms," *International Journal of Engineering Science,* vol. 119, pp. 265-277, 2017.

[8] L. Li, X. Li, and Y. Hu, "Free vibration analysis of nonlocal strain gradient beams made of functionally graded material," *International Journal of Engineering Science,* vol. 102, pp. 77-92, 2016.

[9] F. Ebrahimi and M. R. Barati, "Vibration analysis of nonlocal beams made of functionally graded material in thermal environment," *The European Physical Journal Plus,* vol. 131, p. 279, 2016.

[10] K. Al-Basyouni, A. Tounsi, and S. Mahmoud, "Size dependent bending and vibration analysis of functionally graded micro beams based on modified couple stress theory and neutral surface position," *Composite Structures,* vol. 125, pp. 621-630, 2015.

[11] F. Mehralian and Y. T. Beni, "Vibration analysis of size-dependent bimorph functionally graded piezoelectric cylindrical shell based on nonlocal strain gradient theory," *Journal of the Brazilian Society of Mechanical Sciences and Engineering,* vol. 40, p. 27, 2018.

[12] F. Mehralian, Y. T. Beni, and R. Ansari, "Size dependent buckling analysis of functionally graded piezoelectric cylindrical nanoshell," *Composite Structures,* vol. 152, pp. 45-61, 2016.

[13] H. Zeighampour and Y. T. Beni, "Free vibration analysis of axially functionally graded nanobeam with radius varies along the length based on strain gradient theory," *Applied Mathematical Modelling,* vol. 39, pp. 5354-5369, 2015.

[14] F. Ebrahimi and M. R. Barati, "Thermal environment effects on wave dispersion behavior of inhomogeneous strain gradient nanobeams based on higher order refined beam theory," *Journal of Thermal Stresses,* vol. 39, pp. 1560-1571, 2016.

[15] L. Li, Y. Hu, and L. Ling, "Flexural wave propagation in small-scaled functionally graded beams via a nonlocal strain gradient theory," *Composite Structures,* vol. 133, pp. 1079-1092, 2015.

[16] M. Z. Nejad and A. Hadi, "Non-local analysis of free vibration of bi-directional functionally graded Euler–Bernoulli nano-beams," *International Journal of Engineering Science,* vol. 105, pp. 1-11, 2016.

[17] L.-H. Ma, L.-L. Ke, Y.-Z. Wang, and Y.-S. Wang, "Wave propagation in magneto-electro-elastic nanobeams via two nonlocal beam models," *Physica E: Low-dimensional Systems and Nanostructures,* vol. 86, pp. 253-261, 2017.

[18] M. Akbarzadeh Khorshidi and M. Shariati, "An investigation of stress wave propagation in a shear deformable nanobeam based on modified couple stress theory," *Waves in Random and Complex Media,* vol. 26, pp. 243-258, 2016.

[19] M. Arefi and A. Zenkour, "Analysis of wave propagation in a functionally graded nanobeam resting on visco-Pasternak's foundation," *Theoretical and Applied Mechanics Letters,* vol. 7, pp. 145-151, 2017.

[20] M. Arefi and A. M. Zenkour, "Wave propagation analysis of a functionally graded magneto-electro-elastic nanobeam rest on Visco-Pasternak foundation," *Mechanics Research Communications,* vol. 79, pp. 51-62, 2017.

[21] H. Zeighampour, Y. T. Beni, and M. B. Dehkordi, "Wave propagation in viscoelastic thin cylindrical nanoshell resting on a visco-Pasternak foundation based on nonlocal strain gradient theory," *Thin-Walled Structures,* vol. 122, pp. 378-386, 2018.

[22] H. Zeighampour, Y. T. Beni, and I. Karimipour, "Material length scale and nonlocal effects on the wave propagation of composite laminated cylindrical micro/nanoshells," *The European Physical Journal Plus,* vol. 132, p. 503, 2017.

[23] P. Liu and G.-F. Chen, *Porous materials: processing and applications*: Elsevier, 2014.

[24] S. Iannace and C. B. Park, *Biofoams: Science and applications of bio-based cellular and porous materials*: CRC Press, 2015.

[25] A. Renault, L. Jaouen, and F. Sgard, "Characterization of elastic parameters of acoustical porous materials from beam bending vibrations," *Journal of Sound and Vibration,* vol. 330, pp. 1950-1963, 2011.

[26] M. R. Barati, "On wave propagation in nanoporous materials," *International Journal of Engineering Science,* vol. 116, pp. 1-11, 2017.

[27] M. R. Barati and A. Zenkour, "A general bi-Helmholtz nonlocal strain-gradient elasticity for wave propagation in nanoporous graded double-nanobeam systems on elastic substrate," *Composite Structures,* vol. 168, pp. 885-892, 2017.

[28] R. Rajagopalan and A. Balakrishnan, "Innovations in Engineered Porous Materials for Energy Generation and Storage Applications," ed: CRC Press: Boca Raton, FL, USA, 2018.

[29] P. H. Mareze, E. Brandão, W. D. A. Fonseca, O. M. Silva, and A. Lenzi, "Modeling of acoustic porous material absorber using rigid multiple micro-ducts network: Validation of the proposed model," *Journal of Sound and Vibration,* vol. 443, pp. 376-396, 2019.

[30] D. Chen, J. Yang, and S. Kitipornchai, "Free and forced vibrations of shear deformable functionally graded porous beams," *International Journal of Mechanical Sciences,* vol. 108, pp. 14-22, 2016.

[31] N. Shafiei, S. S. Mirjavadi, B. MohaselAfshari, S. Rabby, and M. Kazemi, "Vibration of two-dimensional imperfect functionally graded (2D-FG) porous nano-/micro-beams," *Computer Methods in Applied Mechanics and Engineering,* vol. 322, pp. 615-632, 2017.

[32] S. S. Mirjavadi, B. Mohasel Afshari, N. Shafiei, S. Rabby, and M. Kazemi, "Effect of temperature and porosity on the vibration behavior of two-dimensional functionally graded micro-scale Timoshenko beam," *Journal of Vibration and Control,* vol. 24, pp. 4211-4225, 2018.

[33] S. S. Mirjavadi, B. M. Afshari, N. Shafiei, A. Hamouda, and M. Kazemi, "Thermal vibration of two-dimensional functionally graded (2D-FG) porous Timoshenko nanobeams," *Steel Compos. Struct,* vol. 25, pp. 415-426, 2017.

[34] F. Z. Jouneghani, R. Dimitri, and F. Tornabene, "Structural response of porous FG nanobeams under hygro-thermo-mechanical loadings," *Composites Part B: Engineering,* vol. 152, pp. 71-78, 2018.

[35] M. Eltaher, N. Fouda, T. El-midany, and A. Sadoun, "Modified porosity model in analysis of functionally graded porous nanobeams," *Journal of the Brazilian Society of Mechanical Sciences and Engineering,* vol. 40, p. 141, 2018.

[36] H. Liu, H. Liu, and J. Yang, "Vibration of FG magneto-electro-viscoelastic porous nanobeams on visco-Pasternak foundation," *Composites Part B: Engineering,* vol. 155, pp. 244-256, 2018.

[37] G.-L. She, K.-M. Yan, Y.-L. Zhang, H.-B. Liu, and Y.-R. Ren, "Wave propagation of functionally graded porous nanobeams based on non-local strain gradient theory," *The European Physical Journal Plus,* vol. 133, p. 368, 2018.

[38] B. Karami and M. Janghorban, "On the dynamics of porous nanotubes with variable material properties and variable thickness," *International journal of engineering science,* vol. 136, pp. 53-66, 2019.

[39] S. Ebrahimi-Nejad, G. R. Shaghaghi, F. Miraskari, and M. Kheybari, "Size-dependent vibration in two-directional functionally graded porous nanobeams under hygro-thermo-mechanical loading," *The European Physical Journal Plus,* vol. 134, p. 465, 2019.

[40] F. Ebrahimi and A. Dabbagh, "Wave dispersion characteristics of heterogeneous nanoscale beams via a novel porosity-based homogenization scheme," *The European Physical Journal Plus,* vol. 134, p. 157, 2019.

[41] F. Ebrahimi, A. Dabbagh, T. Rabczuk, and F. Tornabene, "Analysis of propagation characteristics of elastic waves in heterogeneous nanobeams employing a new two-step porosity-dependent homogenization scheme," *Advances in Nano Research,* vol. 7, pp. 135-143, 2019.

[42] F. Ebrahimi, A. Seyfi, and A. Dabbagh, "A novel porosity-dependent homogenization procedure for wave dispersion in nonlocal strain gradient inhomogeneous nanobeams," *The European Physical Journal Plus,* vol. 134, p. 226, 2019.

[43] M. Mohammadi, M. Safarabadi, A. Rastgoo, and A. Farajpour, "Hygro-mechanical vibration analysis of a rotating viscoelastic nanobeam embedded in a visco-Pasternak elastic medium and in a nonlinear thermal environment," *Acta Mechanica,* vol. 227, pp. 2207-2232, 2016.

[44] F. Ebrahimi and N. Shafiei, "Application of Eringens nonlocal elasticity theory for vibration analysis of rotating functionally graded nanobeams," *Smart Structures and Systems,* vol. 17, pp. 837-857, 2016.

[45] F. Ebrahimi and P. Haghi, "Wave propagation analysis of rotating thermoelastically-actuated nanobeams based on nonlocal strain gradient theory," *Acta Mechanica Solida Sinica,* vol. 30, pp. 647-657, 2017.

[46] M. Shaat, "A general nonlocal theory and its approximations for slowly varying acoustic waves," *International Journal of Mechanical Sciences,* vol. 130, pp. 52-63, 2017.

[47] M. Shaat and A. Abdelkefi, "New insights on the applicability of Eringen's nonlocal theory," *International Journal of Mechanical Sciences,* vol. 121, pp. 67-75, 2017.

[48] S. Faroughi and M. Shaat, "Poisson's ratio effects on the mechanics of auxetic nanobeams," *European Journal of Mechanics-A/Solids,* vol. 70, pp. 8-14, 2018.

[49] S. Gopalakrishnan and S. Narendar, *Wave propagation in nanostructures: nonlocal continuum mechanics formulations*: Springer Science & Business Media, 2013.

[50] S. Gopalakrishnan, *Wave propagation in materials and structures*: CRC Press, 2016.

[51] H. Zeighampour and Y. T. Beni, "Size dependent analysis of wave propagation in functionally graded composite cylindrical microshell reinforced by carbon nanotube," *Composite Structures*, vol. 179, pp. 124-131, 2017.
[52] B. Karami, D. Shahsavari, M. Janghorban, R. Dimitri, and F. Tornabene, "Wave propagation of porous nanoshells," *Nanomaterials*, vol. 9, p. 22, 2019.
[53] M. Eltaher, M. Khater, and S. A. Emam, "A review on nonlocal elastic models for bending, buckling, vibrations, and wave propagation of nanoscale beams," *Applied Mathematical Modelling*, vol. 40, pp. 4109-4128, 2016.
[54] F. Ebrahimi and A. Dabbagh, "Wave propagation analysis of embedded nanoplates based on a nonlocal strain gradient-based surface piezoelectricity theory," *The European Physical Journal Plus*, vol. 132, p. 449, 2017.